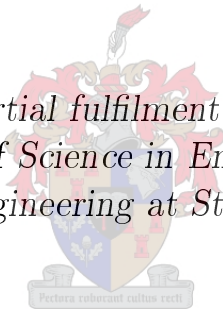


# Accounting for Proof Test Data in a Reliability Based Design Optimisation

by

Maurice Ndashimye

*Thesis presented in partial fulfilment of the requirements for  
the degree of Master of Science in Engineering (Mechanical)  
in the Faculty of Engineering at Stellenbosch University*



Supervisor: Prof. Gerhard Venter

March 2015

# Declaration

By submitting this thesis electronically, I declare that the entirety of the work contained therein is my own, original work, that I am the sole author thereof (save to the extent explicitly otherwise stated), that reproduction and publication thereof by Stellenbosch University will not infringe any third party rights and that I have not previously in its entirety or in part submitted it for obtaining any qualification.

Signature: .....  
M. Ndashimye

Date: .....  
12 September 2014

Copyright © 2015 Stellenbosch University  
All rights reserved.

# Abstract

## Accounting for Proof Test Data in a Reliability Based Design Optimisation

M. Ndashimye

Thesis: MScEng (Mech)

March 2015

Recent studies have shown that considering proof test data in a Reliability Based Design Optimization (RBDO) environment can result in design improvement. Proof testing involves the physical testing of each and every component before it enters into service. Considering the proof test data as part of the RBDO process allows for improvement of the original design, such as weight savings, while preserving high reliability levels.

Composite Over-Wrapped Pressure Vessels (COPV) is used as an example application of achieving weight savings while maintaining high reliability levels. COPVs are light structures used to store pressurized fluids in space shuttles, the international space station and other applications where they are maintained at high pressure for extended periods of time. Given that each and every COPV used in spacecraft is proof tested before entering service and any weight savings on a spacecraft results in significant cost savings, this thesis put forward an application of RBDO that accounts for proof test data in the design of a COPV.

The method developed in this thesis shows that, while maintaining high levels of reliability, significant weight savings can be achieved by including proof test data in the design process. Also, the method enables a designer to have control over the magnitude of the proof test, making it possible to also design the proof test itself depending on the desired level of reliability for passing the proof test.

The implementation of the method is discussed in detail. The evaluation of the reliability was based on the First Order Reliability Method (FORM) supported by Monte Carlo Simulation. Also, the method is implemented in a versatile way that allows the use of analytical as well as numerical (in the form of finite element) models. Results show that additional weight savings can be achieved by the inclusion of proof test data in the design process.

# Uittreksel

## Die Gebruik van Proeftoetsdata in Betroubaarheids Gebaseerde Optimering

*(“Accounting for Proof Test Data in a Reliability Based Design Optimisation”)*

M. Ndashimye

Tesis: MScIng (Meg)

Maart 2015

Onlangse studies het getoon dat die gebruik van ontwerp spesifieke proef-toets data in betroubaarheids gebaseerde optimering (BGO) kan lei tot 'n verbeterde ontwerp. BGO behels vele aspekte in die ontwerpgebied. Die toevoeging van proeftoets data in ontwerpsoptimering bring te weë; die toetsing van 'n ontwerp en onderdele voor gebruik, die aangepaste en verbeterde ontwerp en gewig-besparing met handhawing van hoë betroubaarsheidsvlakke. 'n Praktiese toepassing van die BGO tegniek behels die ontwerp van drukvatte met saamgestelde materiaal bewapening. Die drukvatontwerp is 'n ligte struktuur wat gebruik word in die berging van hoë druk vloeistowwe in bv. in ruimtetuie, in die internasionale ruimtestasie en in ander toepassings waar hoë druk oor 'n tydperk verlang word. Elke drukvat met saamgestelde materiaal bewapening wat in ruimtevaartstelsels gebruik word, word geproeftoets voor gebruik. In ruimte stelselontwerp lei massa besparing tot 'n toename in loonvrag.

Die tesis beskryf 'n optimeringsmetode soos ontwikkel en gebaseer op 'n BGO tegniek. Die metode word toegepas in die ontwerp van drukvatte met saamgestelde materiaal bewapening. Die resultate toon dat die gebruik van proeftoets data in massa besparing optimering onderhewig soos aan hoë betroubaarheidsvlakke moontlik is. Verdermeer, die metode laat ook ontwerpers toe om die proeftoetsvlak aan te pas om sodoende by ander betroubaarheidsvlakke te toets.

In die tesis word die ontwikkeling en gebruik van die optimeringsmetode uiteengelê. Die evaluering van betroubaarheidsvlakke is gebaseer op 'n eerste orde betroubaarheids-tegniek wat geverifieer word met talle Monte Carlo simulasiere resultate. Die metode is ook so geskep dat beide analitiese sowel as eindige element modelle gebruik kan word. Ten slotte, word 'n toepassing

getoon waar resultate wys dat die gebruik van die optimeringsmetode met die insluiting van proeftoets data wel massa besparing kan oplewer.

# Acknowledgements

I would like to express my gratitude to my supervisor Prof. Gerhard Venter for the useful comments, remarks and engagement through the learning process of this master thesis. Furthermore I would like to thank the African Institute for Mathematical Science(AIMS) and the Department of Mechanical Engineering for their financial support.

# Dedications

*This thesis is lovingly dedicated to my mother, Félicité Mukarugira.*

# Contents

<b>Declaration</b>	<b>i</b>
<b>Abstract</b>	<b>ii</b>
<b>Uittreksel</b>	<b>iii</b>
<b>Acknowledgements</b>	<b>v</b>
<b>Dedications</b>	<b>vi</b>
<b>Contents</b>	<b>vii</b>
<b>List of Figures</b>	<b>x</b>
<b>List of Tables</b>	<b>xii</b>
<b>1 Introduction</b>	<b>1</b>
1.1 Background . . . . .	1
1.2 Objectives . . . . .	2
1.3 Thesis Overview . . . . .	3
<b>2 Literature Review</b>	<b>4</b>
2.1 Introduction to Reliability Based Design Optimisation (RBDO)	4
2.1.1 Deterministic Design . . . . .	5
2.1.2 RBDO . . . . .	6
2.2 Reliability Analysis . . . . .	9
2.2.1 Monte Carlo Simulation . . . . .	9
2.2.2 Analytical Approximation Methods . . . . .	10
2.3 System Reliability . . . . .	10
2.3.1 Parallel Systems . . . . .	11
2.3.2 Series Systems . . . . .	12
2.4 Reliability Accounting for Proof Test Data . . . . .	13
2.5 Conditional Reliability . . . . .	14
2.6 Implicit Limit State Functions . . . . .	16
2.7 Composite Over-wrapped Pressure Vessels (COPV) . . . . .	17
2.7.1 Introduction to COPV . . . . .	17



2.7.2	COPV Design Requirements . . . . .	20
2.7.3	Finite Element Model of a COPV . . . . .	21
<b>3</b>	<b>Deterministic Design of a Composite Over-wrapped Pressure Vessel (COPV)</b>	<b>24</b>
3.1	Design Requirements . . . . .	25
3.2	The Analytical Model . . . . .	26
3.2.1	Design Variables . . . . .	26
3.2.2	Objective Function . . . . .	26
3.2.3	Environmental Influence on Composite Structures . . . . .	26
3.2.4	Design Constraints . . . . .	27
3.2.5	Optimisation Process . . . . .	30
3.3	Finite Element Model . . . . .	33
3.3.1	Geometry . . . . .	33
3.3.2	Finite Elements . . . . .	34
3.3.3	Loads and Boundary Conditions . . . . .	35
3.3.4	Composite Material Definition . . . . .	35
3.3.5	Material Properties of Elements . . . . .	39
3.3.6	Analysis . . . . .	39
3.3.7	Optimisation Process . . . . .	39
3.4	Comparison of Analytical Model and Finite Element Model Results . . . . .	40
<b>4</b>	<b>Reliability Based Design Optimisation (RBDO) of a Composite Over-wrapped Pressure Vessel (COPV)</b>	<b>42</b>
4.1	Evaluation of the Probability of Failure . . . . .	42
4.2	Analytical Model . . . . .	45
4.3	Finite Element Model . . . . .	46
4.4	Comparison of Analytical Model and FEM . . . . .	47
<b>5</b>	<b>Proof Test Data Driven RBDO of a COPV</b>	<b>48</b>
<b>6</b>	<b>Conclusions</b>	<b>51</b>
6.1	Overview . . . . .	51
6.2	Future Work . . . . .	52
	<b>Appendices</b>	<b>54</b>
<b>A</b>	<b>The First Order Reliability Method (FORM)</b>	<b>55</b>
<b>B</b>	<b>The Second Order Reliability Method (SORM)</b>	<b>59</b>
<b>C</b>	<b>Finite Difference Method</b>	<b>62</b>
<b>D</b>	<b>Calculation of the Composite Overwrap Thickness and Weight</b>	<b>63</b>

<i>CONTENTS</i>	ix
<b>E Determination of the Winding Angle</b>	<b>68</b>
<b>F Micromechanical Analysis of Laminates</b>	<b>70</b>
<b>G Genz Algorithm</b>	<b>75</b>
<b>List of References</b>	<b>77</b>

# List of Figures

2.1	Reliability evaluation of a load - resistance design optimisation . . .	5
2.2	Probability integration surface and contours in original space (Du, 2005). . . . .	8
2.3	Series and parallel systems . . . . .	11
2.4	Strength distribution after proof testing . . . . .	13
2.5	Reliability evaluation of a load - resistance design optimisation with proof test data . . . . .	14
2.6	Pressure vessel loaded by internal pressure (Mian <i>et al.</i> , 2013) . . .	18
2.7	Typical COPV . . . . .	19
3.1	COPV dimensions . . . . .	25
3.2	Strength decay model parameters(Reeder, 2012) . . . . .	29
3.3	Distribution of starting points in the design space . . . . .	32
3.4	Sorted optimal weights . . . . .	32
3.5	Geodesic profile . . . . .	34
3.6	Geometry of the COPV . . . . .	34
3.7	COPV QUAD4 mesh . . . . .	35
3.8	Composite layup . . . . .	37
3.9	Path of the fibre . . . . .	37
3.10	Change in winding angles along the axial direction . . . . .	38
3.11	Von Mises stresses in the composite shell of the deterministic design	40
4.1	MPP recursive search method . . . . .	43
4.2	Flowchart of the FORM method. . . . .	44
5.1	Trade-off graph between the proof test magnitude and the probability of failing the proof test. . . . .	50
A.1	Probability integration surface in reduced standard normal space (Du, 2005). . . . .	56
A.2	Most probable point . . . . .	58
B.1	Rotation of coordinates . . . . .	60
B.2	Comparison of FORM and SORM . . . . .	61

*LIST OF FIGURES*

xi

D.1	Nomogram for the estimation of the weight of geodesic domes (Peters <i>et al.</i> , 2011) . . . . .	67
E.1	Winding angle for geodesic domes (Peters <i>et al.</i> , 2011) . . . . .	68
F.1	Deformation in longitudinal direction (Yadama and Englund, 2007)	71
F.2	Deformation in transverse direction (Yadama and Englund, 2007) .	72
F.3	Deformation in a volume element (Yadama and Englund, 2007) . .	73
F.4	Shearing deformation in a volume element (Yadama and Englund, 2007) . . . . .	73

# List of Tables

2.1	COPV design requirements . . . . .	21
3.1	COPV design specifications . . . . .	25
3.2	Normal distributions of design parameters . . . . .	31
3.3	Results of the analytical deterministic design . . . . .	33
3.4	Carbon-Epoxy composite material properties . . . . .	36
3.5	Results of the FEM design . . . . .	39
3.6	Comparison of results for deterministic designs . . . . .	40
4.1	Results of the analytical RBDO design . . . . .	46
4.2	Individual probabilities of failure for the deterministic and the RBDO designs . . . . .	46
4.3	Results of FEM based RBDO design . . . . .	47
4.4	Comparison of results for RBDO design . . . . .	47
D.1	Value of the parameter $c$ . . . . .	67

# Chapter 1

## Introduction

### 1.1 Background

RELIABILITY Based Design Optimisation (RBDO) methods have been investigated over the past few decades. They are currently considered to be important design methods since almost all engineering problems present as there is a certain level of uncertainty in the parameters of almost all engineering problems. In RBDO processes, reliability indices for each of the failure modes of a system are calculated and those reliability indices are then used to estimate the overall probability of failure of the system.

In various areas of engineering such as aerospace, a limited number of components are manufactured and weight reductions are extremely important. In some cases, where high levels of safety are required like NASA for example, each and every component is proof tested before being used. A new RBDO approach proposed by Venter and Scotti (2010) has shown that the consideration of the proof test data in the design process can allow further weight savings without loss of the overall reliability of the component.

In this thesis, this RBDO method that accounts for proof test data is applied to the design and life estimation of a Composite Over-wrapped Pressure Vessel (COPV). The aim is to illustrate the method and prove that the method is better than the more traditional methods. In the thesis the versatility of the method is explored by implementing the method using an analytical model of a COPV in the first instance, then a Finite Element Model (FEM) of the COPV for more accuracy and flexibility.

COPVs are lighter structures than all metal pressure vessels. They are mostly used as fuel storage tanks on-board spacecraft. Pressurised fluids contained in COPVs have the potential of causing fatal accidents if they are released suddenly due to the failure of the vessel. Design standards for COPVs have been developed over the past four decades. Until now, there is no deterministic mechanism to determine the life span of a COPV because it can fail at an unanticipated time due to stress rupture.

Stress rupture is a failure mode of COPVs as a result of composite degrada-

tion. Stress rupture depends on the stress in the composite, the temperature and the period of time the COPV stays loaded. This degradation results in a sudden structural failure of the COPV. The stress rupture can occur while the COPV is maintained at stress levels below its ultimate strength for an extended period of time. The stress rupture failure mechanism is complex, not well understood, and difficult to predict accurately (McLaughlan and Forth, 2011).

In this study, a reliability-based design method is applied to the design of COPVs in order to ensure that the COPV will remain reliable at a stress level set by the designer for a period of time also defined at the design stage. For this reason, the stress rupture of COPVs is modelled using the Strength Decay Model (SDM) developed by Reeder (2012). The model is based on the concept that the strength of fibres in the overwrap of the COPV deteriorates over time. Stress rupture occurs when the decayed strength falls below the level of the applied stress.

## 1.2 Objectives

The two main objectives of this project are namely:

1. The implementation of the RBDO method that accounts for proof test data.
2. Application of the method to the design of a real engineering component that has been designed using other standard design methods, in order to prove the advantages of the newly developed method over the existing design methods.

The design of a COPV has been chosen as the application of the method. The design tool that was developed in this study will allow for the use of both an analytical model and a Finite Element Model (FEM) of the vessel. The vessel is designed using deterministic methods and reliability-based design methods with consideration of proof test data and without consideration of proof test data. Results are then compared to prove the benefits of including proof test data in the design process.

The main objectives are accomplished through the completion of the following steps,

- Become familiar with the current techniques used for optimisation and simulation in industry.
- Become familiar with finite element modelling software (SimXpert, Patran).
- Become familiar with the Python programming environment.

- Implement the RBDO method that accounts for proof test data using Python with the option of coupling it with finite element analysis tools (Nastran).
- Become familiar with the design of COPVs.
- Apply the RBDO method that accounts for proof test data to the design of COPVs and compare the method to standard design methods used in industry.

### 1.3 Thesis Overview

This thesis is composed of six chapters laid out as follows,

- Chapter 1 is an introduction in which there is a brief background of the project and its objectives.
- Chapter 2 is a literature review on which the subsequent sections are built. The literature review explains in a broad way RBDO, the inclusion of proof test data in the design process and the design of COPVs.
- In Chapter 3 the focus is on the deterministic design of a COPV. In this chapter two design approaches, one using an analytical model and another using a finite element model are applied to the design of a COPV, results of both methods are then compared and discussed.
- In Chapter 4 RBDO of a COPV is further discussed, two models of the COPV are again used, an analytical model and a finite element model.
- In Chapter 5 the focus is on the consideration of proof test data in a RBDO environment of COPVs. Again, two models of the COPV are considered.
- In Chapter 6 conclusions are presented and recommendations for further studies are made.



# Chapter 2

## Literature Review

Design is one of the major components of engineering. Along with the quick advancement in computational technology, engineering design also keeps growing at a remarkable pace. Powerful computers have enabled the design of new tools that can handle complex engineering problems with large numbers of parameters. They have also enabled designers to achieve a higher level of accuracy using modelling and simulations. In this chapter an insight into engineering design is provided with focus on Reliability Based Design Optimisation (RBDO) that accounts for proof test data. Also, the design of Composite Overwrapped Pressure Vessels (COPVs) is reviewed with the objective to use it as an illustrative example in subsequent chapters.

### 2.1 Introduction to Reliability Based Design Optimisation (RBDO)

Engineering design consists of sizing components of a system so that the whole system satisfies defined criteria of performance, cost, durability and safety. However, in most cases the design process is not straightforward due to the existence of uncertainties in parameters of the design that needs to be accounted for. The basic formulation of an engineering design optimisation problem is the determination of a set of design variables that maximises or minimises a system performance function while satisfying a set of system performance constraints.

Most designers assume that design variables are deterministic and account for uncertainties that exist in modelling, simulation, manufacturing processes and uncertainties in system usage such as extreme loads and structural strength degradation over time by means of safety factors. This type of design is referred to as deterministic design. In contrast, in a reliability based design environment, all uncertain parameters of the design problem are considered as random variables, and uncertainties in design variables are directly taken into consideration using appropriate probability distributions.

### 2.1.1 Deterministic Design

In a deterministic design optimisation, the aim is to define a set of values that minimise the performance function and at the same time satisfy constraints imposed on the system to be designed, such as maximum load, failure stress and so on.

Typically, a deterministic design problem is formulated as (Vanderplaats, 1984):

$$\begin{aligned} \text{Minimise: } & f(\mathbf{x}) \\ \text{such that: } & g_i(\mathbf{x}) \leq 0 \quad i = 1, m \\ & x_i^{lower} \leq x_i \leq x_i^{upper} \quad i = 1, n \end{aligned} \quad (2.1.1)$$

where  $\mathbf{x}$  is a vector of  $n$  design variables,  $f(\mathbf{x})$  is the objective function,  $g_i$  is the  $i^{th}$  constraint that models the  $i^{th}$  failure mode of the system out of  $m$  failure modes and  $x_i^{lower}$  and  $x_i^{upper}$  are respectively lower and upper boundaries on the design variables. All equations and variables in this formulation are deterministic. Uncertainties in variables are taken into consideration using safety factors.

Safety factors are determined depending on the level of reliability that needs to be achieved and the nature of the problem. Let us use the Load and Resistance Factor Design (LRFD) method to illustrate the deterministic design optimisation. As illustrated in Fig. 2.1, the load  $L$  and the resistance  $R$  are both random variables with probability density functions  $f_L(L)$  and  $f_R(R)$ , with mean  $\mu_L$  and  $\mu_R$  and standard deviation  $\sigma_L$  and  $\sigma_R$  respectively. The shaded area on the graph, which is the overlap between the curves of probability distributions of the load and the resistance represents the probability of failure.

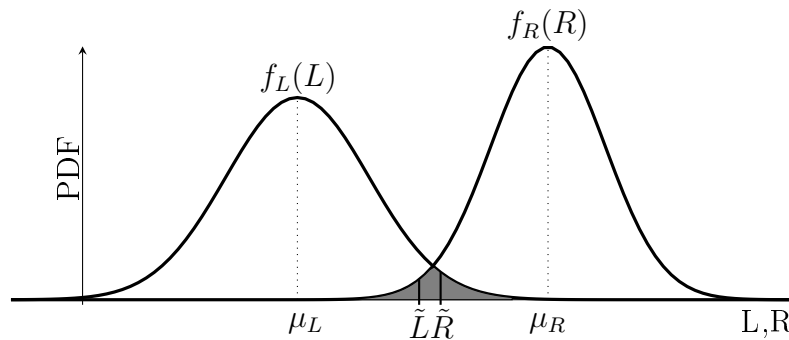


**Figure 2.1:** Reliability evaluation of a load - resistance design optimisation

According to Haldar and Mahadevan (2000) there are three factors that influence the size of the overlap between the two curves,

1. The positions of the curves relative to each other, that is, the means of the two variables. Increasing the distance between the two curves reduces the overlap.
2. The dispersion of the two curves, that is the standard deviations of the two variables. Small values of standard deviations will result in narrow curves and small overlap.
3. The shapes of the curves, that is, the probability distribution function.

The goal of design optimisation is to find optimal values that reduce the overlap region as much as possible. The deterministic design approach reduces the risk of failure by shifting the positions of the curves. This is achieved by using safety factors. The approach is to make sure that the nominal resistance  $\tilde{R}$  is greater than the nominal load  $\tilde{L}$  by a safety factor defined as

$$SF = \frac{\tilde{R}}{\tilde{L}} \quad (2.1.2)$$

The nominal resistance  $\tilde{R}$  and the nominal load  $\tilde{L}$  are deterministic values obtained from statistical analysis. Data for the analysis can be obtained by performing tests on components or using values provided in data logs. The nominal resistance is a fixed value smaller than the mean resistance. It is calculated to be below the mean resistance by the product of deviation and a correction factor referred to as a K-factor.

$$\tilde{R} = \mu_R - k_R \sigma_R \quad (2.1.3)$$

In the same way, the nominal design load is a fixed value taken above the mean load. It is calculated to be the sum of the mean load and the product of a correction factor and the standard deviation. Applying the safety factor to the load, the final expression of the design load is,

$$\tilde{L} = SF(\mu_L + k_L \sigma_L) \quad (2.1.4)$$

The safety factor can be applied to the load, to the resistance or to both.

### 2.1.2 RBDO

In deterministic design optimisation described in the previous section, all design parameters of the system are deterministic, and uncertainties are taken into account by means of safety factors. This approach often leads to over-designing some parts of the system and eventually under-designing others. A rigorous method of designing reliable systems is the individual consideration of uncertainties in design parameters, that is, using random variables to define the parameters of the system instead of deterministic values, and designing a

system that has reliability standards that have been defined by the designer beforehand.

In the RBDO framework, a design model can generally be defined as (Haldar and Mahadevan, 2000):

$$\begin{aligned} & \text{Minimise: } f(\mathbf{x}) \\ & \text{such that: } P(F) \leq P_f \\ & \quad x_i^{lower} \leq x_i \leq x_i^{upper} \quad i = 1, n \end{aligned} \quad (2.1.5)$$

where  $\mathbf{x}$  is a vector of  $n$  design variables,  $f(\mathbf{x})$  is the objective function,  $P(F)$  is the probability of system failure  $F$ ,  $P_f$  is the maximum probability of failure allowed for the design,  $x_i^{lower}$  and  $x_i^{upper}$  are respectively the upper and lower boundaries on the design variables.

In most instances, engineering systems have to satisfy more than one criterion or constraint related to each of its failure modes, and the evaluation of the system reliability is a combination of more than one probability of failure. The combination of individual probabilities of failure into a system probability of failure depends on many factors. According to Haldar and Mahadevan (2000) the most predominant factors are the following:

1. The contribution of each of the individual failure events to the system failure
2. The statistical correlation between individual failure events
3. Post failure status at the component level and system level
4. Parallelism in the system
5. Progressive failure of components.

For an individual failure mode,  $F_i$ , the probability of failure is,

$$P(F_i) = P(G_i \leq 0) \quad (2.1.6)$$

where  $G_i$  is the limit-state surface, or failure surface which represents a state beyond which the structure can no longer fulfil the function for which it was designed. The probability of failure is then calculated as,

$$P_f = \int \dots \int_{g(X_1, X_2, \dots, X_n) \leq 0} f(X_1, X_2, \dots, X_n) dX_1 dX_2 \dots dX_n \quad (2.1.7)$$

where  $f(X_1, X_2, \dots, X_n)$  is the joint probability density function for the basic random variables  $X_1, X_2, \dots, X_n$ . This expression is often referred to as

the probability integral over the failure set, and  $1 - P_f$  is referred to as the reliability.

$$1 - P_f = \int \dots \int_{g(X_1, X_2, \dots, X_n) > 0} f(X_1, X_2, \dots, X_n) dX_1 dX_2 \dots dX_n \quad (2.1.8)$$

The corresponding reliability index is

$$\beta = \Phi^{-1}(1 - P_f) \quad (2.1.9)$$

where  $\Phi$  is the standard normal distribution function, and  $\Phi^{-1}$  its inverse. The probability integrations in Eq. A.0.1 and Eq. 2.1.8 are visualised with a two-dimensional case in Fig. 2.2.

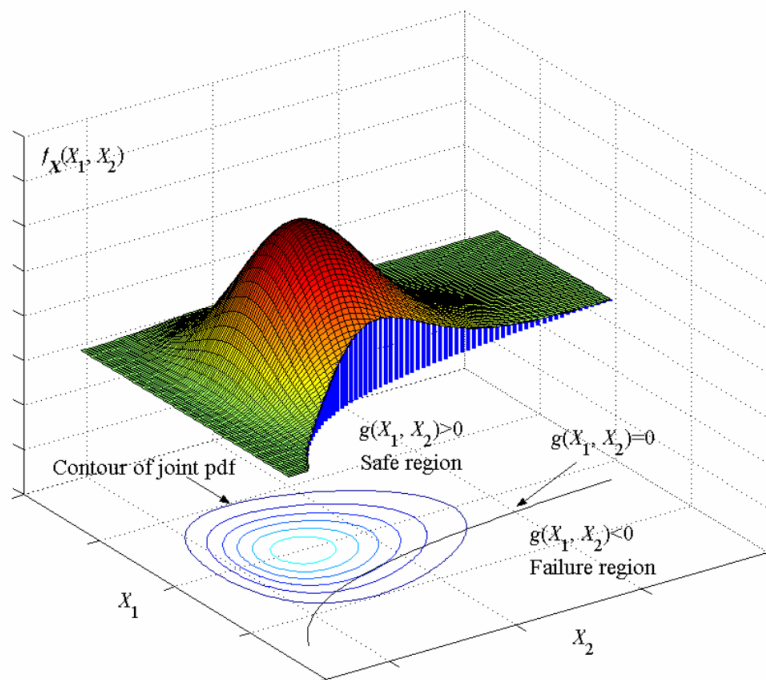


**Figure 2.2:** Probability integration surface and contours in original space (Du, 2005).

All the points on the contours have the same probability density. Note that generally contours are not circular. The limit state  $g(X_1, X_2)$  is also plotted on the  $X_1, X_2$  plane. The probability integrations in Eq. A.0.1 and Eq. 2.1.8 are the volumes underneath the surface of the joint probability density function  $f(X_1, X_2)$ , in the failure region and safe region respectively.

## 2.2 Reliability Analysis

Direct evaluation of the probability integration is extremely difficult due to the fact that firstly, the integration is multidimensional, the dimensionality is typically high for engineering applications. Secondly, the integrand  $f(X_1, \dots, X_n)$ , which is the joint probability distribution function, is generally non-linear. Lastly, the integration boundary  $g(X_1, \dots, X_n)$  is in general non-linear and multidimensional.

The easiest method commonly used to estimate the reliability in structural engineering is the Standard Monte Carlo simulation technique (SMC) (Olsson *et al.*, 2002). SMC techniques have the advantage of being simple to understand and to execute, they give solutions which converge towards the exact probability of failure, when a sufficient number of simulations are carried out. The drawback is that for small values of probability often encountered in structural engineering, the amount of computation time required is prohibitively large.

In most cases, a reasonable approach is to use analytical approximations of Eq. A.0.1. The first and second order reliability methods are the most widely used analytical methods. The advantage of the analytical methods is that, they often do not require large computation time. The drawback is that they do not provide exact results for the failure probabilities, but only approximations.

A suitable method is the one which gives acceptable estimates of the probability at an acceptable computational cost. Therefore, the choice of a method has to be justified. The justification may be based on a verification of the method by another relevant method. Analytical methods can generally be verified by simulation methods, which are considered as verified if a sufficient number of experiments are carried out.

### 2.2.1 Monte Carlo Simulation

Monte Carlo simulation refers to any technique of statistical sampling used to approximate solutions to quantitative problems. Any problem modelled using random variables represented by their respective probability distribution functions, can be simulated using the Monte Carlo method. This is achieved by simulating the full system many times, each time randomly choosing a value for each variable from its probability distribution.

To evaluate the failure or reliability of an engineering system with a limit-state represented by Eq. A.0.1, all the random variables in the equation are assumed to be statistically independent. The Monte Carlo simulation consists of drawing samples of the variables according to their probability distribution density functions and feeding them into the equation  $g(X_1, X_2, \dots, X_n)$ . The event of failure is realised when the drawn sample yields  $g(X_1, X_2, \dots, X_n) < 0$ . Let  $N_f$  be the number of simulations where  $g(X_1, X_2, \dots, X_n) < 0$  and  $N$  the total number of simulations. The estimated probability of failure is then

$$P_f = \frac{N_f}{N} \quad (2.2.1)$$

The accuracy of Monte Carlo simulation depends on the number of iterations used in the simulation process. One way of evaluating the accuracy of the method is the calculation of the coefficient of variation (COV) of the estimated probability of failure. The COV is a dimensionless value defined as the ratio of the standard deviation to the mean.

Assuming that the simulation is a sequence of  $N$  independent Yes/No experiments depending on whether  $g(X_1, X_2, \dots, X_n) < 0$  or not, the Monte Carlo Simulation can be considered as an experiment counting the number of failures in a sample of size  $N$  drawn with replacement, and the number of failures out of  $N$  trials can be considered to follow a binomial distribution. The coefficient of variance of a binomial distribution for a Monte Carlo process is then given by the expression

$$COV(P_f) = \frac{\sqrt{\frac{(1 - P_f)P_f}{N}}}{P_f} \quad (2.2.2)$$

where  $P_f$  is the estimated probability of failure. Therefore, a sufficient number of simulation cycles should satisfy the relation

$$N \geq \frac{1 - P_f}{P_f COV(P_f)^2}. \quad (2.2.3)$$

Commonly a coefficient of variation of 10% is used for engineering problems (Li *et al.*, 2013) and the sufficient number of simulation cycles can be estimated to be greater than  $\frac{100}{P_f}$ .

## 2.2.2 Analytical Approximation Methods

The direct evaluation of the probability integral being cumbersome, the evaluation of reliability requires approximations. Depending on the shape of the failure region, a first order or a second order Tylor series approximation of the limit state function may be used. Methods developed based on these approximations are referred to as First Order Reliability Method (FORM) and Second Order Reliability Method (SORM) respectively, they are the most widely used approximation methods in reliability analysis. A broad discussion of both methods is presented in Appendix A and Appendix B.

## 2.3 System Reliability

Up to this point, we have explored reliability analysis for a single failure mode or limit state function. Real life problems are presented in the form of systems which are collections of components connected together to perform a function for which the system is designed with a certain level of reliability.

System reliability depends on the reliabilities of the individual components of the system, as well as the way the components are interconnected within the system. In most cases, relationships between components are complex and difficult to be understood fully.

In a reliability analysis environment, relationships between components are modelled depending on the contribution of components to the system failure event. In cases where the system failure occurs when any of the components fail, the system is referred to as a series system (or a weak link system) and the system failure is defined by the union of individual component failures.

$$P(F_s) = P(F_1 \cup F_2 \cdots \cup F_n) \quad (2.3.1)$$

Alternatively, if the system failure occurs after the failure of all the components, the system is referred to as a parallel system (or redundant system) and the system failure is defined by the intersection of the individual components failures. Fig. 2.3 illustrates series and parallel systems.

$$P(F_p) = P(F_1 \cap F_2 \cdots \cap F_n) \quad (2.3.2)$$

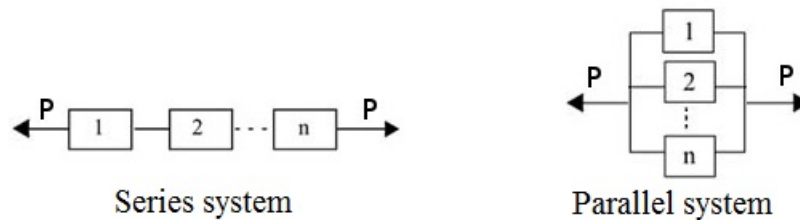


**Figure 2.3:** Series and parallel systems

In general, engineering systems are defined by a combination of series and parallel subsystems.

### 2.3.1 Parallel Systems

In the standard normal space, the probability of failure of a parallel system is evaluated using the integral

$$P(F_p) = \frac{1}{\sqrt{(2\pi)^n |\mathbf{cor}|}} \int_{\beta_n}^{\infty} \cdots \int_{\beta_1}^{\infty} \exp \left[ -\frac{1}{2} \mathbf{U}^T \mathbf{cor}^{-1} \mathbf{U} \right] dU_1 \dots dU_n \quad (2.3.3)$$

where  $\mathbf{cor}$  is the correlation matrix, an  $n \times n$  matrix made of coefficients of correlation between individual components of the system.

The analytical evaluation of Eq. 2.3.3 is extremely difficult for large number of variables as is the case in reliability analysis of engineering systems. Alternatively the integral can be evaluated using numerical integration, approximating



the answer or bounding the answer. Numerical integration is efficient when the number of variables is lower than 500 (Venter and Scotti, 2010). In this thesis, a numerical integration algorithm developed by Genz (1992) is used to evaluate the probability of failure of parallel systems numerically.

### 2.3.2 Series Systems

The series system probability of failure cannot directly be evaluated using Eq. 2.3.3. The integral represents the intersection of individual failure modes, and the series system probability is defined by the union of failure modes.

To evaluate the series system reliability, the expression of system reliability is transformed into an expression that uses intersections. There are two possible ways to transform the expression of the series system into an expression that uses intersections. The first approach is to express the probability of failure  $F_s$  in terms of its complement  $\bar{F}_s$  as

$$P(F_s) = 1 - P(\bar{F}_s) = P(\overline{F_1 \cup F_2 \cdots \cup F_n}) \quad (2.3.4)$$

Then using the De Morgan's rule (Haldar and Mahadevan, 2000) the expression is further transformed into

$$P(F_s) = 1 - P(\bar{F}_1 \cap \bar{F}_2 \cap \cdots \cap \bar{F}_n) \quad (2.3.5)$$

The right side of Eq. 2.3.5 can now be evaluated using Eq. 2.3.3. A second alternative is the use of probability mathematics to express unions in terms of intersections, as an example of a two components series system the expression will be transformed as

$$P(F_1 \cup F_2) = P(F_1) + P(F_2) - P(F_1 \cap F_2) \quad (2.3.6)$$

and for a three component series system the expression will be transformed as

$$\begin{aligned} P(F_1 \cup F_2 \cup F_3) = & P(F_1) + P(F_2) + P(F_3) - P(F_1 \cap F_2) - P(F_1 \cap F_3) \\ & - P(F_2 \cap F_3) + P(F_1 \cap F_2 \cap F_3) \end{aligned} \quad (2.3.7)$$

Again after transformation, the expressions obtained are sums of which the terms are either probability of failure of individual components of the system which can be easily evaluated or probability of failure of intersections of two or more components which can be evaluated using Eq. 2.3.3.

The first approach has the advantage of having just one multivariate integral but the subtraction of numbers that are very close to each other can cause loss of accuracy. The second approach has the disadvantage that the number of terms grows exponentially with an increase of the number of failure modes. In the second approach, the sum of probability of failure of individual failure modes is the most important part of the sum. An upper limit to the

probability of failure can be obtained by just considering these terms with the advantage of evaluating only univariate integrals. In this case the probability of failure of the system will be estimated by

$$P(F_s) = \min \left( 1, \sum_{i=1}^n P(F_i) \right) \quad (2.3.8)$$

## 2.4 Reliability Accounting for Proof Test Data

Reliability of a design is the probability that the strength of the designed system is higher than the load that will be applied to it. As explained in previous sections and illustrated in Fig. 2.1, the probability of failure represents the overlap between the distributions of load and strength.

A proof test is a non-destructive test performed before a newly designed system enters service. During a proof test the system is basically subjected to loads that exceed its operational load to prove that the system is safe and can operate within the design margins.

After the proof test, the probability of failure becomes a conditional probability of failure which is the probability of failure given that the system has successfully passed the proof test. In this study the assumption that the system has passed the proof test successfully is used. This means that we assume that the system does not fail the proof test and the system continues to be fully functional after the proof test. Graphically, a successful proof test cuts off the tail of the strength distribution (Venter and Scotti, 2010) as illustrated in Fig. 2.4.

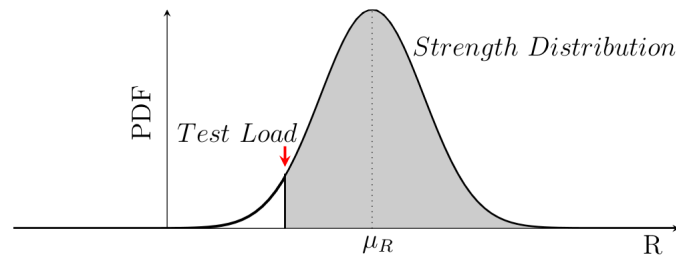


**Figure 2.4:** Strength distribution after proof testing

The conditional probability of failure is represented by the shaded area in Fig. 2.5. The proof test reduces the probability of failure, this reduction in probability of failure can be quantified and included in the design process (Venter and Scotti, 2010).

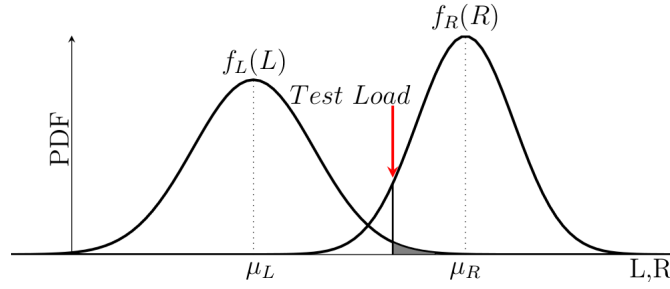


**Figure 2.5:** Reliability evaluation of a load - resistance design optimisation with proof test data

The RBDO optimisation problem defined in Eq. 2.1.5 using the probability of failure  $P(F)$  then becomes

$$\begin{aligned}
 &\text{Minimise: } f(\mathbf{x}) \\
 &\text{such that: } P(F|A) \leq P_f \\
 &\quad 1 - P(A) \leq P_{proof} \\
 &\quad x_i^{lower} \leq x_i \leq x_i^{upper} \quad i = 1, n \\
 &\quad p_j^{lower} \leq p_j \leq p_j^{upper} \quad j = 1, np
 \end{aligned} \tag{2.4.1}$$

where  $A$  represents the event of passing the proof test,  $1 - P(A)$  is the probability of failing the proof test,  $P_f$  is the maximum probability of failure allowed for in the design,  $P_{proof}$  is the maximum allowable probability of failing the proof test and  $p_j$  are magnitudes of the components of the proof load.

In this RBDO optimisation formulation, the designer fixes the probability of failing the proof test depending on implications of failing the proof test. For example, for a structural design, where failing the proof test is not costly, the designer can allow higher risk of failing the proof test and get significantly higher weight savings, and in cases where the cost of failing the proof test is high, the designer can prefer successful proof tests over weight savings.

In addition, this RBDO method allows the designer to have control over the proof test. In fact, the design has variables that describe the magnitude of the proof test loads, therefore, the designer is empowered with the ability to design the system and the proof test simultaneously.

## 2.5 Conditional Reliability

The conditional probability is the probability of occurrence of an event given that another event occurred, this is called the probability multiplication rule. Haldar and Mahadevan (2000) states that

$$P(A \cap B) = P(A|B)P(B) \tag{2.5.1}$$

where  $P(A|B)$  is the conditional probability, from the multiplication rule, the conditional probability can be calculated as

$$P(A|B) = \frac{P(A \cap B)}{P(B)} \quad (2.5.2)$$

Therefore, for a single mode of failure and a single proof test, the conditional probability of failure given that the design has passed the proof test successfully, is

$$P(F|A) = \frac{P(F \cap A)}{P(A)} \quad (2.5.3)$$

The numerator and the denominator of this fraction are evaluated using the integral 2.3.3 for  $n = 2$  and  $n = 1$  respectively. The integrals are computed using the Genz algorithm.

A system conditional probability of failure implies the consideration of multiple failure modes and multiple proof tests. Again the system can be a parallel system or a series system.

For a parallel system, the condition probability of failure is given by

$$P(F_p|A) = \frac{P(F_p \cap A)}{P(A)} = \frac{(P(F_1 \cap F_2 \cap \dots \cap F_{nf}) \cap P(A_1 \cap A_2 \cap \dots \cap A_{np}))}{P(A_1 \cap A_2 \cap \dots \cap A_{np})} \quad (2.5.4)$$

In this case the numerator is evaluated using the Eq. 2.3.3 for  $n = nf + np$  where  $nf$  is the number of system failure modes and  $np$  the number of proof tests. The denominator is also evaluated using the Eq. 2.3.3 for  $n = np$ . Both integrals can be computed using the Genz algorithm.

For a series system, the condition probability of failure is given by

$$P(F_s|A) = \frac{P(F_s \cap A)}{P(A)} = \frac{(P(F_1 \cup F_2 \cup \dots \cup F_{nf}) \cap P(A_1 \cap A_2 \cap \dots \cap A_{np}))}{P(A_1 \cap A_2 \cap \dots \cap A_{np})} \quad (2.5.5)$$

In this case only the denominator can be directly evaluated using the integral 2.3.3 for  $n = np$ , the numerator has to be transformed to have only intersections, the two approaches used to calculate the series system probability of failure introduced in Section 2.3.2 are applicable. The first approach that uses the complement and the De Morgan Rule gives

$$\begin{aligned} P(F_s|A) &= 1 - \frac{P(\overline{F_p} \cap A)}{P(A)} \\ &= 1 - \frac{(P(\overline{F_1} \cap \overline{F_2} \cap \dots \cap \overline{F_{nf}}) \cap P(A_1 \cap A_2 \cap \dots \cap A_{np}))}{P(A_1 \cap A_2 \cap \dots \cap A_{np})} \end{aligned} \quad (2.5.6)$$

The second approach uses the mathematics of probability to express unions using intersections, for example, a system conditional probability of failure with two failure modes will be transformed as

$$P(F_s|A) = \frac{P(F_1 \cup F_2) \cap A}{P(A)} = \frac{P(F_1 \cap A)}{P(A)} + \frac{P(F_2 \cap A)}{P(A)} - \frac{P(F_1 \cap F_2 \cap A)}{P(A)} \quad (2.5.7)$$

After transformation using either approach the final expressions can be evaluated using the integral 2.3.3 then computed using Genz algorithm.

Using numerical experimentation, Venter and Scotti (2010) found that the first approach is more computationally involved than the second approach. This is due to the fact that the Genz algorithm doesn't converge easily for the integration of the numerator of Eq. 2.5.6. On the other hand, they have found that, although the number of terms on the right hand side of Eq. 2.5.7 could be large, the Genz algorithm converges easily for all of these terms. Also, using the second approach, the upper bound of  $P(F_s|A)$  given by

$$P(F_s|A) = \min \left( 1, \sum_{i=1}^{nf} P(F_i|A) \right) \quad (2.5.8)$$

can be used to approximate  $P(F_s|A)$  without significant loss of accuracy. Therefore, the second approach was used in this project.

## 2.6 Implicit Limit State Functions

In previous sections we discussed the evaluation of the probability of failure assuming that a differentiable limit state function is available. However, in most engineering problems an analytical limit state function is not available. The performance function is commonly computed using numerical methods such as finite element analysis, dynamic simulation or computational fluid dynamics.

In a situation where the limit state is not available reliability can be evaluated using three approaches (Haldar and Mahadevan, 2000): Monte Carlo simulation, approximation of the limit state and uncertainty analysis.

Monte Carlo simulation has been introduced in Subsection 2.2.1 using explicit limit state functions. The same approach can be used for implicit limit state functions provided that there is a possibility of changing the input values of the numerical method used to compute the limit state of the system. Again, the method becomes highly computationally expensive for small values of probability of failure.

The approximation of implicit limit states is carried out collecting data using a few simulations in the estimated neighbourhood of the MPP. Then a first or second order polynomial is fitted to the data using regression analysis methods such as the least square method. Once the polynomial is available the same techniques used in the case of explicit limit state functions are applicable.

Uncertainty analysis investigates how uncertainty in the output of a numerical model can be allocated to different sources of uncertainty in its inputs. Uncertainty based analysis is in general more efficient compared to the other two methods. In this approach, sensitivities of the limit state are calculated using perturbation methods such as the finite difference method (Haldar and Mahadevan, 2000), iterative perturbation analysis techniques (Ho and Cao,

1991) and the score function or likelihood method (Rubinstein and Shapiro, 1993).

In this thesis, the finite difference method is preferred due to its simplicity and versatility. In the finite difference method, each of the variables is perturbed at a time and the change in the limit state is calculated, the finite difference method is discussed in Appendix ??.

In reliability analysis using implicit limit states FORM is preferred because it requires only first order derivatives. Second order derivatives required in SORM increase computational cost and can be a significant source of errors due to significant round-off errors and series truncations.

## 2.7 Composite Over-wrapped Pressure Vessels (COPV)

### 2.7.1 Introduction to COPV

Pressure vessels are closed containers designed to hold fluids at pressures significantly higher than the ambient pressure. COPVs are formed by an ultra thin walled metal tank that plays the role of a liner over-wrapped by a composite composed of continuous high tensile fibres that carry the pressure loads combined with cured resin that maintain the fibres in position and carry shear loads.

The first composite pressure vessel was designed in 1919 in an attempt to use gas as fuel for motor cars (Kaempffert, 1919). It was a tank with a 15 cm diameter spirally wound with two layers of steel tape. The domes of the vessel were connected by high tensile strength wires to prevent rupture in the longitudinal direction. The vessel could withstand pressures up to 69 MPa.

Rocket motor cases were the first composite over-wrapped structures that used filament winding technology (Peters *et al.*, 2011). The project was initiated in the cold war when light structures were needed for long range missiles. Any weight savings could be used to increase either the range of the missile or its payload.

The first filament wound COPV was made in the 1970's when the NASA Fire-fighter's Breathing System Program requested the industry to manufacture a lightweight and higher-pressure compressed air vessel. A glass fibre COPV weighing half the weight of the existing metal vessel was suggested. The COPV received certification in 1975, and commercial production was initiated. Since then, the COPV technology has matured and fibre technology has expanded from glass to Kevlar and Carbon composites leading to further weight reductions.

COPVs are made by winding a band of fibres impregnated with wet resin around a mandrel and curing it. Fibre reinforced structures are particularly attractive in applications where weight savings are crucial such as avia-

tion and aerospace applications because of their high directional strength and stiffness-to-density ratios. Especially, fibre-reinforced composites are suited for COPV, mainly because the loads in cylindrical pressure vessel are inherently anisotropic, that is, the loads in the hoop direction  $\sigma_h$  are double the loads in the axial direction  $\sigma_a$  and the loads are dominated by tension as can be seen in Fig. 2.6.

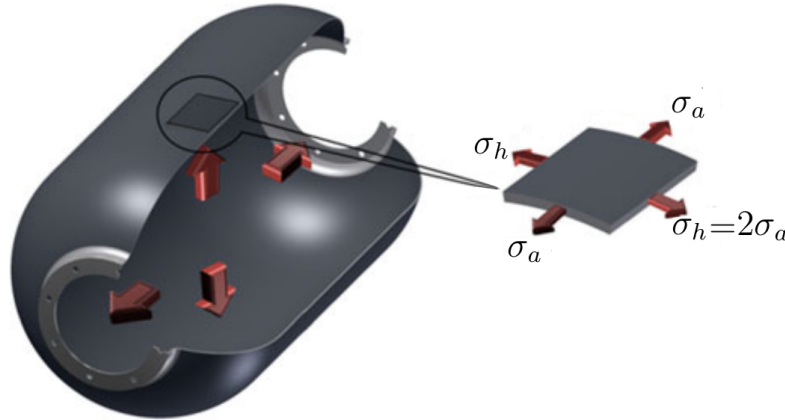


**Figure 2.6:** Pressure vessel loaded by internal pressure (Mian *et al.*, 2013)

In applications where weight savings are crucial, COPVs are preferred to the widely used isotropic all-metal pressure vessels because of their higher pressure vessel efficiency  $\eta$  (Kaushik *et al.*, 2004) defined by the equation,

$$\eta = \frac{PV}{W} \quad (2.7.1)$$

where  $P$ ,  $V$  and  $W$  are the burst pressure of the vessel, its volume and its weight respectively. The use of COPVs allow weight savings in the range of 30% to 50% compared to all-metal pressure vessels (McLaughlan and Forth, 2011). Typical COPVs are shown in Fig. 2.7.



**Figure 2.7:** Typical COPV

Pressurising the COPV may cause cracks in the resin matrix and cause leakage of the fluids contained in the vessel. To prevent leakage COPVs are lined with rubber, plastic or ultra thin metals. Also, during the manufacturing process, the liner is used as a mandrel over which the composite is wrapped. In some cases the liner is strong enough to share part of the load with the composite over-wrap and is called a load-sharing liner.

COPVs are designed to contain large amounts of energy that can cause fatal accidents if released instantly. NASA has identified four major failure modes of COPVs (McLaughlan and Forth, 2011) as listed below, along with measures that are taken in order to mitigate the failure.

1. Burst from over-pressurisation. This failure mode is mitigated by proof-testing the vessel and controlling the pressurisation source.
2. Fatigue failure of the liner, mitigated by visual observation of liners to eliminate liners with significant flaws. Also, proper safety factors are used while defining the vessel cycle life.
3. Burst from damage, mitigated using proper protection from damage and visual inspection of surface damages before pressurisation.
4. Stress rupture of the composite. Unlike isotropic metal vessels, COPV can fail due to static fatigue or stress rupture of the fibres in the composite. This is a sudden failure of the COPV that occurs if it has been maintained below its maximum operating pressure for a long period of time. The failure is the result of degradation of the fibres over time. It cannot be detected by current technology. Experiments have shown that stress rupture depends on time, pressure and temperature. Using experimental data, it has been shown that stress rupture can be predicted using Weibull distributions (Lorie *et al.*, 2006). In this thesis, stress rupture is modelled using the strength decay model developed by Reeder (2012).



## 2.7.2 COPV Design Requirements

A standard COPV is made of an ultra thin metallic liner over-wrapped with reinforcing fibres and an epoxy matrix. It can be regarded as a shell of revolution, covered by a net with a particular pattern that depends on how it has been wound. Typical loads applied to a COPV consist of internal pressure,  $P$ , and externally applied axial load,  $F_a$ , resulting from the vessel interfacing with other structural components.

Conceptually, pressure vessels can have any shape, however, due to manufacturability issues, surface of revolution such as cylinders, cones and sections of spheres are preferred shapes for pressure vessel designers. The most popular shape of pressure vessels is a cylinder with two dome shaped end caps referred to as domes. The shape of the domes is chosen depending on the fibre winding pattern. The most effective winding pattern is the geodesic winding pattern in which the fibres follow geodesic paths which are the shortest distances between the tangent lines where the cylindrical part of the vessel ends, and the polar openings of the vessel. Geodesic patterns of fibres have an influence on the shape of the dome. The shaping of a geodesic dome is explained in subsequent sections.

The design of the COPV is driven by its geometric limits, operational requirements, ultimate structural loads and stiffness, environmental requirements such as temperature and the required overall reliability of the vessel. COPV design parameters are given in Table 2.1 along with typical values that those parameters can take.

**Table 2.1:** COPV design requirements

Parameters	Typical values
Geometry:	
Length	67.6 cm
Diameter	42.2 cm
Operational requirements:	
Operating pressure	30 MPa
Minimum burst pressure	37.5 MPa
Proof test pressure	45 MPa
Tank weight	13.5 kg
Internal volume	65 l
Pressurant	He, O <sub>2</sub> , ...
Shell leakage	10 <sup>-6</sup> scc/s
Interface structural strength:	
Compression	-525 kN/m
Tension	+470 kN/m
Shear and torsion	±350 kN/m
Bending stiffness	2.9 × 10 <sup>9</sup> N/m <sup>2</sup>
Environment requirement:	
Temperature	-95°C to 60°C
Humidity	100% RH
Life span	> 10 years
Safety factors:	
Proof factor	1.25
Minimum burst	1.5
Material requirement	
Metals	Aluminium, Titanium, ...
Fibre	Kevlar, Carbon
Epoxy	Epon 826, Cyanate ester, ...
Reliability	0.9999

### 2.7.3 Finite Element Model of a COPV

COPVs are shells of revolution, if the composite is quasi-isotropic and the vessel is subjected to an axisymmetric loading, it can be modelled using an axisymmetric finite element model, otherwise, it is modelled using a three dimensional finite element model. In case a 3D model is chosen, its geometry is either imported as a CAD model or drawn by revolving the profile of the

COPV around its axis. The angle of revolution can be  $90^\circ$ ,  $180^\circ$  or  $360^\circ$  depending on whether a quarter model, a half model or a full model is desired.

The profile of a COPV depends on the choice of the shape of the dome which can be spherical, ellipsoidal, geodesic and so on. Equations that define various shapes are available, they are used to generate lists of  $(x, y, z)$  coordinates of points which are then connected using cubic splines to get a smooth curve. The profile of the cylindrical part of the COPV is obtained by drawing a line that connects the curves describing the domes. Depending on whether both domes have the same shape or not, it might be necessary to model the full vessel or just half of it using adequate symmetries.

After defining the geometry, the next step is the definition of the composite overwrap layout. The composite is considered a layered orthotropic material, each layer having a different thickness and winding angle. In practice, there are two types of layers, helical layers and hoop layers. Helical layers cover the entire vessel and they are balanced, that is, for every layer with a winding angle  $\alpha$ , there is a corresponding layer with a winding angle  $-\alpha$  (SIMULIA, 2007). The winding angle and thickness of helical layers are not uniform.

The winding angle varies according to Eq. 2.7.2 (SIMULIA, 2007)

$$\alpha(r) = \sin^{-1} \left( \frac{r_0}{r} \right) \pm \delta \left( \frac{r - r_0}{r_{tl} - r_0} \right)^n \quad (2.7.2)$$

where  $\alpha(r)$  is the wind angle at radius  $r$ ,  $r_0$  is the radius at the helical turnaround point,  $r_{tl}$  the radius at the dome-cylinder tangent line. The thickness varies according to Eq. 2.7.3 (SIMULIA, 2007)

$$t(r) = \frac{r_{tl} t_{tl} \cos(\alpha_{tl})}{\left( r + 2BW \left( \frac{r_{tl} - r}{r_{tl} - r_0} \right)^4 \right) \cos(\alpha(r))} \quad (2.7.3)$$

where  $t(r)$  is the thickness at radius  $r$ ,  $t_{tl}$  the thickness of helical layer at the tangent line,  $\alpha_{tl}$  is the wind angle at the tangent line, and  $BW$  the winding band width. Hoop layers cover only the cylindrical part of the vessel, they have a uniform thickness and they are wound at  $90$  degrees reference taken from the axis of the vessel.

A COPV model is meshed using shell elements to which ply material properties are assigned. Ply materials are defined considering each of the layers composing the overwrap separately and assigning to them 2D-orthotropic material properties, orientation angles and thicknesses.

Loads applied to a COPV finite element model are internal pressure, thermal loads and axial loads originating from the interaction of the vessel with other structural components. Boundary conditions depend on whether an axisymmetric or 3D model of the vessel is considered. Also, the 3D model can be full, half or quarter depending on the loading of the vessel.

The model as set up is then analysed. The output of a COPV model analysis can be set to give results at ply level referred to as layered results

where stresses and deformations are given for each individual ply. In contrast, the output can be set to give results of the composite as a whole without considering individual plies, these results are referred to as non-layered or global results, they can be averages or maximums of layered results.

## Chapter 3

# Deterministic Design of a Composite Over-wrapped Pressure Vessel (COPV)

The focus of the current study is to demonstrate the benefits of proof test data in Reliability-Based Design Optimisation (RBDO) over other more traditional design methods. The theory underpinning the deterministic and the reliability-based design approaches with and without proof test data, is reviewed in Chapter 2. In this and subsequent chapters we will discuss the application of these design approaches on a real life engineering problem. By comparing results of the three design approaches, we will be able to showcase the benefits of including proof test data in the design process.

The design of COPV has been chosen as an application for the method developed in this project. The chosen COPV was designed by Kawahara and McCleskey (1966) and improved by Tam *et al.* (2002). The vessel has been chosen because it has been manufactured, successfully proof tested and certified for commercialisation.

This chapter is dedicated to the deterministic design of the COPV. The focus is on the optimisation of the composite overwrap. The liner is considered to be as thin as possible, and therefore does not contribute to the structural strength and is thus not included in the optimisation process. To ensure that the current design is realistic, the original design of the COPV was used as a benchmark.

At the beginning of the chapter the design requirements are specified, this is followed by a detailed design optimisation of the COPV. Two designs are carried out, one is based on an analytical model of the COPV and the other on its finite element model. The comparison of the results of the two designs as well as the comparison of both results to the original design will be provided at the end of this chapter.

### 3.1 Design Requirements

The COPV is designed to hold 67.3 litre of Helium at a pressure of 3.1 MPa and a temperature of 60°C. The COPV was proof tested by pressurising it at a pressure 1.25 times its operating pressure. The proof test pressure is referred to as proof pressure in subsequent sections. The minimum burst pressure, that is the maximum internal pressure the COPV can withstand, is estimated to be 1.5 times its operating pressure. Detailed requirements are provided in Table 3.1 and in Fig. 3.1 .

**Table 3.1:** COPV design specifications

Parameter	Requirement
Maximum Operating Pressure	3.1 MPa
Proof Pressure	3.875 MPa
Minimum Burst Pressure	4.65 MPa
Size	422 mm dia. × 676 mm length
Tank Weight	13.4 kg maximum
Operating Temperature	−95.5°C to 60°C
Fibres	Carbon T1000
Resin	Epoxy
Winding Pattern	Geodesic

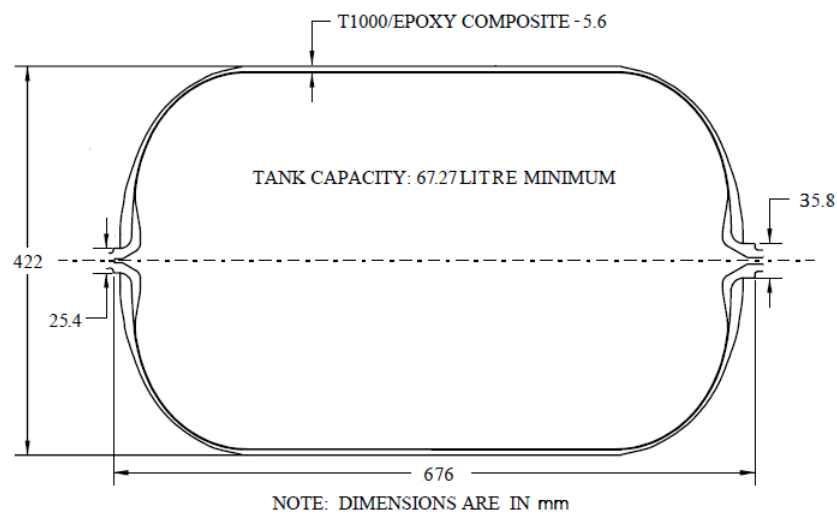


**Figure 3.1:** COPV dimensions

## 3.2 The Analytical Model

An optimisation problem as described in Eq. 2.1.1, consists of minimising (or maximising) a function of the design variables referred to as the objective function taking into account some limitations or constraints on the system to be designed. The objective function as well as the constraints can be mathematical equations that express the performance of the system and its limitations. In this case, the model of the system is referred to as an analytical model. Alternatively, the role of these mathematical expressions can be played by black-box software such as finite element models or computational fluid dynamics models. In this section, the optimisation of a COPV based on its analytical model is presented.

### 3.2.1 Design Variables

The design of the COPV has two types of parameters. The first type involves pre-assigned parameters that are defined as requirements by the design. These are, the inner radius of the cylindrical part of the vessel  $R$ , the length of the cylindrical part  $L_{cyl}$ , the maximum operating pressure  $P$ , radii of the forward and aft polar openings of the vessel respectively  $R_{E\_FWD}$  and  $R_{E\_AFT}$ , the material to be used as well as the winding technique that will be used to build the vessel. In the current design, a geodesic winding is considered. All these parameters are defined in Table 3.1. The second type involves design variables, of which the values are the outcome of the optimisation. The variables of a COPV design are the thickness of the hoop windings and the thickness of the helical windings.

### 3.2.2 Objective Function

The optimisation of a COPV is concerned with maximising its internal volume and maximum allowable pressure while minimising its weight. In the current study the internal volume of the vessel and its operating pressure are predefined parameters, therefore, the objective function is the weight of the pressure vessel. The calculation of the thickness and weight of the composite and the determination of the winding angle are discussed in Appendix D.

### 3.2.3 Environmental Influence on Composite Structures

The design of composite structures takes into consideration the influence of external factors such as changes in temperatures, humidity and corrosive agents since they can affect mechanical performance of the structure by changing its physical properties (Gosavi *et al.*, 2014).

Elevated temperatures can decrease the strength of the structure by thermal softening. In this project, the influence of thermal softening was neglected because we consider all the loads to be carried by fibres longitudinally loaded,

and experiments have shown that the longitudinal strength and tensile modulus of a unidirectional composite ply remains almost for temperatures ranging from  $-120^{\circ}\text{C}$  to  $-120^{\circ}\text{C}$  (Gosavi *et al.*, 2014; Nettles and Biss, 1996).

Composite matrices can absorb moisture by exposure to humid environments. The moisture enters through the surface and then diffuses through the matrix and can affect the mechanical performance of the composite. This environmental influence on the composite can be avoided using special coatings that reduce moisture absorption.

### 3.2.4 Design Constraints

Constraints applied to the design originate from the requirements related to the maximum strength of the vessel, the life span of the vessel and its preferred failure modes. These constraints will be elaborated on one by one.

#### 3.2.4.1 Structural Integrity

Composite material failure characterisation is still debatable unlike the status of failure characterisation for isotropic materials. The two failure theories that are widely adopted for isotropic materials, namely the Von Mises Criterion and the Tresca Criterion are not applicable to composite materials (Christensen, 2005) simply because both theories predict that the uni-axial tension and compression will be the same and both are independent of a superimposed mean normal stress.

A number of theories for composite failure characterisation are available, amongst others, the maximum stress criterion, the Tsai-wu criterion and the Tsai-Hill are widely used in laminate composite (Christensen, 2005). In this thesis, the Tsai-Wu criterion is used.

The Tsai-Wu failure criterion is given by the equation (Wu and Tsai, 1971)

$$\left(\frac{1}{X_t} - \frac{1}{X_c}\right)\sigma_1 + \left(\frac{1}{Y_t} - \frac{1}{Y_c}\right)\sigma_2 + \frac{\sigma_1^2}{X_t X_c} + \frac{\sigma_2^2}{Y_t Y_c} + 2F_{12}\sigma_1\sigma_2 + \frac{\sigma_{12}^2}{S^2} < 1 \quad (3.2.1)$$

where  $\sigma_1$  and  $\sigma_2$  are respectively stresses in the axial (1) and transverse (2) directions of the fibres.  $X$  and  $Y$  are respectively strengths in the axial and transverse directions, subscripts  $t$  and  $c$  stand for tension and compression respectively,  $S$  is the shear strength and

$$F_{12} = -\frac{1}{2}\sqrt{\frac{1}{X_t X_c Y_t Y_c}} \quad (3.2.2)$$

#### 3.2.4.2 Life Span of the Vessel

Experimental data show that a COPV can fail after a certain period of time if it is maintained at a lower pressure than the acceptable operating pressure



(McLaughlan and Forth, 2011). This phenomenon is referred to as stress rupture. It is thus crucial to include the time to failure in the design process and design a structure that will last long enough for the application for which it is designed.

A COPV that fails as a result of stress rupture does not present any apparent signs like leakage or cracks before the failure occurs. Stress rupture is thus an unpredictable and an unanticipated failure mode of COPVs. From experiments, it has been shown that stress rupture is a function of the stresses in the composite, the operating temperature and the time (Murthy and Phoenix, 2009; Pat B. McLaughlan *et al.*, 2011).

To mitigate stress rupture, COPVs are maintained at pressures much lower than their burst pressure, typically less than half the burst pressure (Pat B. McLaughlan *et al.*, 2011). Also, reliability models developed based on existing data are used to predict the likelihood of stress rupture (Lorie *et al.*, 2006). However, models used to date don't account directly for the initial strength of the fibre, they simply model the life span of the fibre depending on their loading and operating conditions.

In this thesis, a model developed by Reeder (2012) under the assumption that the pressure vessel material is factory-made with an initial strength  $S_0$  that deteriorates over time, was used. The model is referred to as the strength decay model. However, the initial strength cannot be specified with certainty because the strength of the fibres varies from one spool to the next and there is no technique available to date that can be used to measure the initial strength of a fibre in a COPV without destroying it.

The strength of fibres wound on a loaded COPV will decay until falling below the value of the applied stress, causing the failure of the COPV. In the strength decay model, the fibre strength at any instant of time  $T$  before the time of failure  $T_f$  is given by

$$s(T) = \sigma \left( 1 - \frac{T - T_f}{d} \right)^{1/b} \quad (3.2.3)$$

where  $b$  is a shape parameter of the strength decay curve and  $d$  is a scaling parameter that scales the rate of the strength decrease.

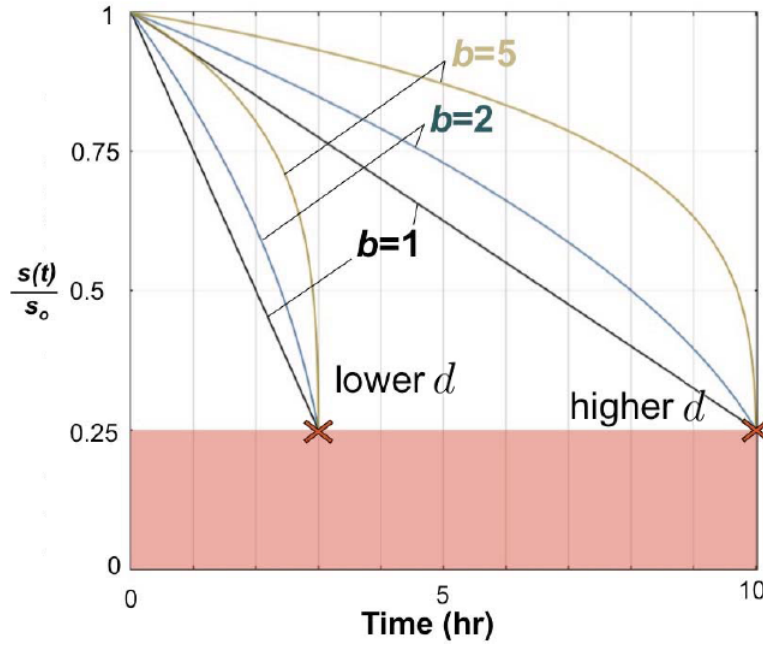


Figure 3.2: Strength decay model parameters(Reeder, 2012)

As can be seen from Fig. 3.2,  $b = 1$ , results in a linear strength decay curve, and for larger values of  $b$  the strength decay curve tends to be constant with a faster decrease as the strength approaches the value of the applied stress. The shape of the curve fits the behaviour of stress rupture, where the COPV does not show any signs of weakness until it fails suddenly. It can also be seen from Fig. 3.2 that the bigger the value of  $d$ , the longer the COPV life span. Constants  $b$  and  $d$  are intrinsic properties of materials; they are determined comparing the strength decay material with experimental data (Reeder, 2012). At the instant  $T_0 = 0$ , the strength  $s(T_0) = s_0$ . Plugging these values in Eq. 3.2.3 we get

$$\frac{s_0}{\sigma} = \left(1 + \frac{T_f}{d}\right)^{1/b} \quad (3.2.4)$$

Assuming that the COPV is subjected to a constant uniform loading throughout its life span, the time to failure will be given by

$$T_f = d \left( \left( \frac{s_0}{\sigma} \right)^b - 1 \right) \quad (3.2.5)$$

Reliability methods such as FORM, Eq. 3.2.5 can be used to estimate the probability that a COPV loaded at a constant stress  $\sigma$  will fail after a period of time  $T_f$ . However, the initial strength  $s_0$  in Eq. 3.2.5 is unknown and cannot be estimated with certainty, it can only be represented by a random variable  $S$  of which the distribution is established through testing or using existing data available in data logs.

For carbon fibres (IM6), the strength decay model parameters as deduced from data analysis are  $b = 0.04$  hr and  $d = 147$  (Reeder, 2012). Typically, COPVs are designed to last at least ten years in service, which means  $T_f = 87658$  hours. The life span constraint is thus expressed as,

$$d \left( \left( \frac{s_0}{\sigma} \right)^b - 1 \right) > 87658 \quad (3.2.6)$$

### 3.2.4.3 Preferred Failure Mode of the Structure

A failure of the vessel originating from the hoop windings is preferred compared to a helical failure. The reason a failure in hoop direction is preferred is that it is easily predictable and depends only on the shell loading of the vessel. To ensure that the vessel will fail in the hoop windings, the ratio of the helical fibre stress to the hoop fibre stress is set to be less than one. Typically, the stress ratio is chosen between 60% and 85% (Peters *et al.*, 2011). In this study, we used a stress ratio of 75%. The stress ratio ( $SR$ ) is given by the equation

$$\begin{aligned} SR &< 0.75 \\ \frac{\sigma_x}{\sigma_y} &< 0.75 \end{aligned} \quad (3.2.7)$$

where  $\sigma_x$  is the stress in the axial direction and  $\sigma_y$  the stress in the hoop direction.

## 3.2.5 Optimisation Process

For deterministic optimisation, uncertainties in design parameters are taken into consideration by means of safety factors. According to Eq. 2.1.3 and Eq. 2.1.4, the strength of materials is calculated to be the mean strength reduced by the product of a correction factor and the standard deviation. The correction factor is referred to as the K-factor.

The correction factor depends on the test sample size and the required reliability and level of confidence. In this project a correction factor of 3 and a safety factor of 1.5 are assumed. In practice, it requires 35 tests to obtain a K-factor of 3 for a normally distributed parameter if a reliability of 99% is required with a confidence level of 95% (Venter and Scotti, 2010). It is also assumed that all parameters of the current design are uncorrelated, normally distributed random variables. This assumption is not realistic since parameters like the strength of materials are known to be distributed following an exponential distribution. However, the assumption can be achieved by means of appropriate change of variables (Haldar and Mahadevan, 2000).

Values of the mean and standard deviation (Std Dev) representing the normal distribution for each of the design parameters are provided in Table 3.2. Note that for the thicknesses, only the standard deviation value is given. The

reason is that, these parameters are not predefined and will be obtained as a result of the optimisation process.

The standard deviation for the thickness has been chosen to be in the order of the thickness of two plies which is about 0.2 mm. The standard deviation of the pressure is likely to be small due to the existence of accurate loading facilities; it is assumed to be 5%. For the strength of materials, it has been found from experiments that a deviation of 12% exists in measurements (Duell *et al.*, 2008). The standard deviation in the time to failure is likely to be large; it is chosen to be 50%. For the winding angle, a standard deviation of 10% is assumed.

**Table 3.2:** Normal distributions of design parameters

Parameter	Unity	Mean	Std Dev
Thickness of hoop plies ( $t_h$ )	m	–	$2 \times 10^{-4}$
Thickness of helical plies ( $t_a$ )	m	–	$2 \times 10^{-4}$
Pressure(P)	Pa	$3.1 \times 10^6$	$1.55 \times 10^5$
Winding angle( $\alpha$ )	°	6	0.6
Time to failure ( $T_f$ )	Hours	87660	43830
Longitudinal tensile strength( $X_t$ )	Pa	$1.5 \times 10^9$	$0.18 \times 10^9$
Transverse tensile strength( $Y_t$ )	Pa	$40 \times 10^6$	$4.8 \times 10^6$
Longitudinal compressive strength( $X_c$ )	Pa	$1.5 \times 10^9$	$0.18 \times 10^9$
Transverse compressive strength( $Y_c$ )	Pa	$246 \times 10^6$	$29.52 \times 10^6$

The optimisation process is carried out using the sequential quadratic programming algorithm (SQP) of the DOT<sup>1</sup> suite. Given that the SQP method is sensitive to the starting point and can be easily trapped in a local minimum, the optimisation is performed for 36 different starting points and the best local solution is chosen. A sampling method based on the translational propagation algorithm (Viana *et al.*) has been used to generate the starting points. The algorithm is based on translations of small building blocks or seeds consisting of one or more points in the design space. The distribution of starting points is represented in Fig. 3.3. Starting points were generated assuming that the thickness is in the range of 1 mm to 5 mm.

<sup>1</sup>Design Optimisation Tools by Vanderplaats Research & Development, Inc. (Vanderplaats Research & Development, 2001)

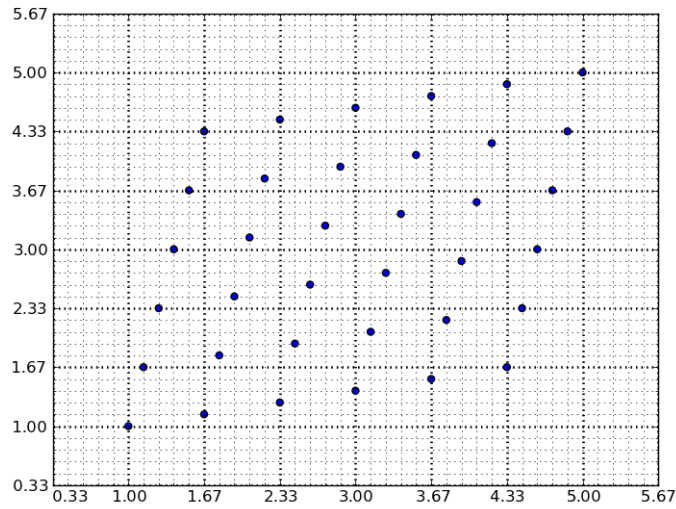


**Figure 3.3:** Distribution of starting points in the design space

A graph of sorted results considering various starting points is represented in Fig. 3.4. The optimal weights are sorted to show how many times the optimisations resulted in a particular local minimum.

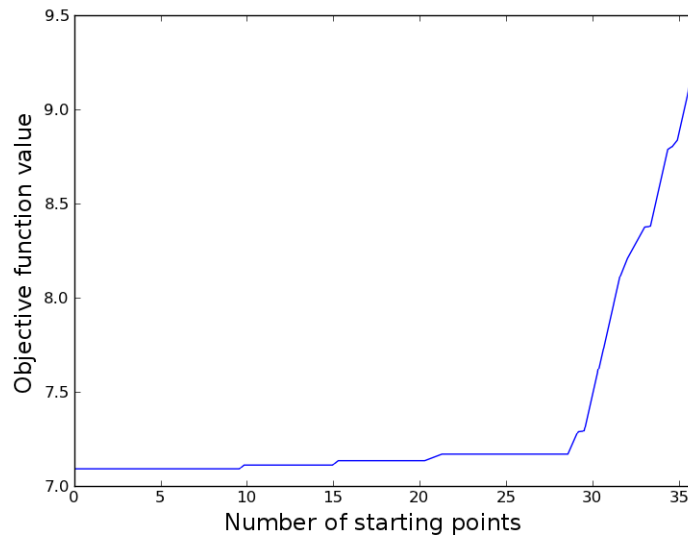


**Figure 3.4:** Sorted optimal weights

For the optimal solution, the optimisation was completed after 5 iterations, the first and the third constraints were active, and none of the constraints were violated. Results are reported in Table 3.3.

**Table 3.3:** Results of the analytical deterministic design

Parameter	Value
$t_h$ (mm)	3.04
$t_a$ (mm)	2.78
$t_{total}$ (mm)	5.82
Weight (kg)	6.52

### 3.3 Finite Element Model

The finite element model of the COPV was created using MSC Patran 2012. The software was chosen because it features the MSC Laminate Modeller, a tool which has a wide range of options for composite material creation. An in depth discussion of the model creation and analysis is given in subsequent subsections.

#### 3.3.1 Geometry

The geometry of the 1/8 of the COPV was generated by creating its profile, then revolving it through 90 degrees around the axis of symmetry for the vessel. The 1/8 model is preferred because the overwrap of the COPV has an axial symmetry and the only loading that is considered is an internal pressure which is also symmetric about the axis of the COPV.

The ideal shape of the vessel is one which allows all the fibres to be wound in such a way that they will experience a uniform tension throughout their length when the vessel is loaded. This is achieved by designing domes that allow the fibres to be wound following an isotensoid pattern which is achieved by winding the fibres following geodesic paths in the dome parts of the vessel. Also, fibres wound following geodesic paths do not slip during the winding process (Peters *et al.*, 2011) and that contributes to the reduction of void spaces which are air spaces trapped in the composite during the winding process.

A geodesic path is a curve connecting two points on a surface and following the shortest path. The design of a geodesic dome is obtained by creating geodesic lines between the vessel polar opening and the cylindrical part of the vessel. The geodesic dome profile is obtained from the elliptic integral 3.3.1 (Kabir, 2000; Kumar and Kumari, 2012).

$$\bar{z}(\bar{r}^*) = -\sqrt{1 - \bar{r}_0^2} \int_1^{\bar{r}^*} \frac{\bar{r}^3 dr}{\sqrt{\bar{r}^2 - \bar{r}_0^2 - \bar{r}^6 (1 - \bar{r}_0^2)}} \quad (3.3.1)$$

where  $z$  is the axial coordinate,  $r$  the radial coordinate,  $r_0$  the radius of the polar opening, and  $R$  the radius of the cylindrical part.  $\bar{r} = \frac{r}{R}$ ,  $\bar{z} = \frac{z}{R}$  and  $\bar{r}_0 = \frac{r_0}{R}$ . The above elliptic equation has a point of inflection at  $\bar{r} = 1.225r_0$  as illustrated in Fig. 3.5.

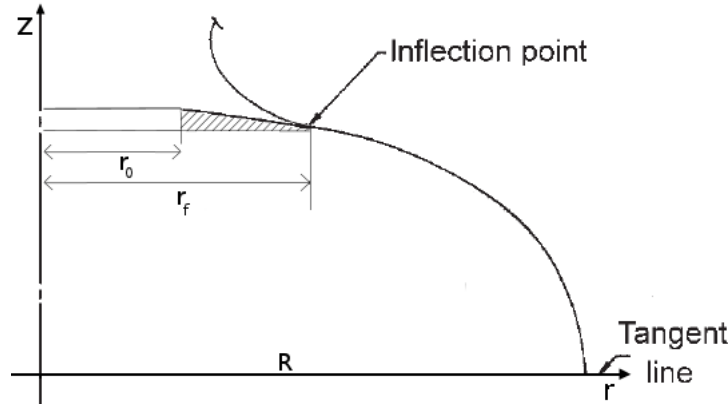


**Figure 3.5:** Geodesic profile

From the inflection point to the opening, another geodesic profile is defined using the following equation (Kumar and Kumari, 2012),

$$\bar{z}(\bar{r}^*) = -\bar{r}_f^2 \sqrt{1 - \bar{r}_0^2} \int_{\bar{r}_f}^{\bar{r}^*} \frac{\bar{r} \sqrt{\bar{r}^2 - \bar{r}_0^2} d\bar{r}}{\sqrt{(\bar{r}_f^2 - \bar{r}_0^2) - \bar{r}_f^4 ((1 - \bar{r}_0^2) \bar{r}^2 (\bar{r}^2 - \bar{r}_0^2))}} + \bar{z}_f \quad (3.3.2)$$

where  $\bar{z}_f = \bar{z}(\bar{r}^* = r_f)$  and  $r_f = 1.225r_0$  is the radius at the point of inflection.

To obtain the profile of the COPV, the centre of the COPV is set to lie at the origin of the coordinates, and Eq. 3.3.1 and Eq. 3.3.2 are integrated considering the radius to be lying on the X coordinates. Since the two openings are not of the same size, each dome is considered separately. The geometry of the vessel is shown in Fig. 3.6.

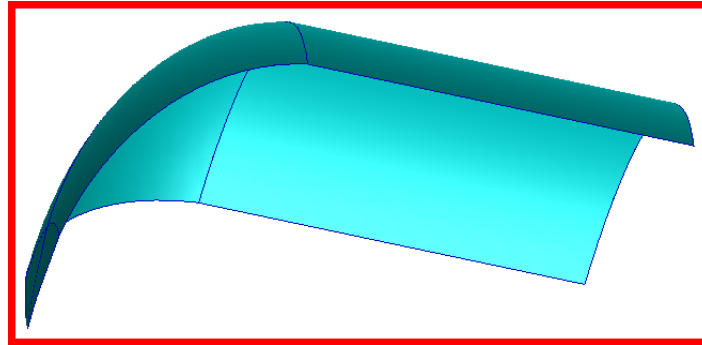


**Figure 3.6:** Geometry of the COPV

### 3.3.2 Finite Elements

The model has been meshed using QUAD4 elements. Mesh seeds are first applied on all curves in order to obtain a uniform mesh. To ensure the convergence of the model, mesh refinement was applied. The final model had 4560 elements in total and 4690 nodes. The mesh is shown in Fig. 3.7

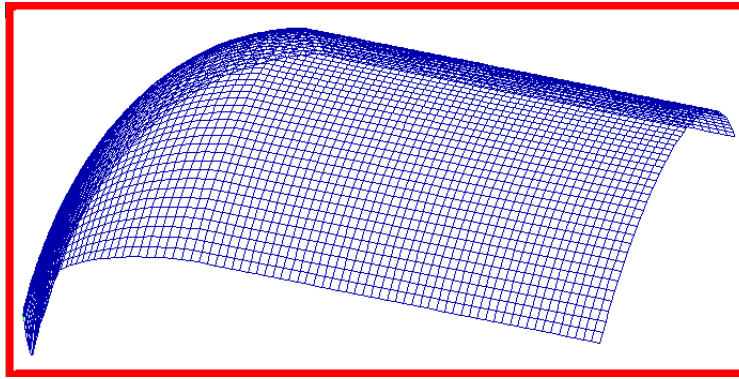


Figure 3.7: COPV QUAD4 mesh

### 3.3.3 Loads and Boundary Conditions

In this study, the only load that is applied to the COPV is the internal pressure. Axial loads due to interfacing between the vessel and other mechanical components, as well as thermal loads are not considered.

The application of loads and boundary conditions is achieved by setting three conditions:

- A uniform pressure of 3.1 MPa applied to all elements of the model.
- Cylindrical coordinates with the  $Z$  axis coinciding with the axis of the vessel are used to create boundary conditions. Edges parallel to the axis of the vessel are fixed in the  $\theta$  direction. The edge perpendicular to the axis of the vessel is fixed in the  $Z$  direction and the polar point fixed in the  $r$  and  $\theta$  directions.

### 3.3.4 Composite Material Definition

Composite material refers to material made by the combination of two or more constituent materials. In material science, the combination of two or more materials can result in a final material that has better structural properties compared to the constituents. Often, composite materials are preferred to homogeneous material because of their high strength, lightness and cost effectiveness.

The definition of composite materials depends on the manufacturing process. The composite in COPV is made of continuous fibres wound over a liner acting as a mandrel. It is composed of many layers wound at different angles. Hoop windings are wound at an angle of  $90^\circ$  reference taken as the axis of the COPV and helical windings are wound at an angle  $\alpha$  measured from the vessel axis. The axial winding angle is calculated using Eq. E.0.2. An angle of  $6^\circ$  is calculated for the current design.



MSC-Laminate Modeler is a PATRAN tool dedicated to the creation of laminated composite material. Three levels of material properties are created successively in order to create laminate material properties (MSC, 2012).

1. Homogeneous materials are created using PATRAN, typically these material are orthotropic, they represent fibres together with resin.
2. Composite materials are created using Patran. Composite materials reference the homogeneous materials and transform them by adding on manufacturing process data such as thickness of plies, initial warp/weft angle and maximum strain. These materials also specify how plies are laid up by specifying a sequence of plies with their respective composite materials, thicknesses and orientations.
3. 2D shell layered material properties are created referencing to the composite material created at the second stage. A reference direction is chosen for plies that have been laid up at the second stage and an application region is chosen. Additional options such as the composite material offset, non-structural weight, reference temperature and others can be specified at this stage.

Homogeneous material properties that represent fibres together with the resin can be deduced from material properties of isotropic fibres and isotropic resin by means of a micro-mechanics analytical method referred to as the rule of mixtures. The rule of mixtures is discussed in Appendix ??.

Composite material properties obtained using the rule of mixtures and material properties for carbon T1000 (Toray, 2008) and Epon 826 (Hexion, 2005) are reported in Table 3.4.

**Table 3.4:** Carbon-Epoxy composite material properties

Property	Unity	Carbon	Epoxy	Composite
Longitudinal modulus ( $E_{11}$ )	GPa	294	2.75	177.5
Transverse modulus ( $E_{22}$ )	GPa	294	2.75	6.8
Shear modulus (G)	GPa	113.08	0.97	2.38
Poisson's ratio ( $\nu_{12}$ )	–	0.3	0.42	0.35
Density ( $\rho$ )	kg/m <sup>3</sup>	1800	1160	1544

After creation of homogeneous materials, the composite layup is created by specifying the orientation of plies relative to a chosen direction, their number and the sequence in which they are stacked on top of each other.

In the current study, the composite needs to be quasi-isotropic. That is, it needs to be equally strong in hoop and helical directions. In order to obtain a quasi-isotropic composite, plies need to be balanced. That means, for each ply wound at an angle  $\alpha$  there is a corresponding ply wound at an angle  $-\alpha$ .

For a COPV, ply sequences on the cylindrical part of the vessel are different from the ply sequences on the domes, the reason being that hoop windings only cover the cylindrical part. Taking the axis of the vessel as a reference and recalling that  $\alpha = 6^\circ$ , plies on the cylindrical part of the current model are stacked in the order  $90^\circ$ ,  $6^\circ$ ,  $-6^\circ$ ,  $90^\circ$  as illustrated in Fig. 3.8. Each ply has a thickness of 0.1 mm and 56 plies are used for a total thickness of 5.6 mm.

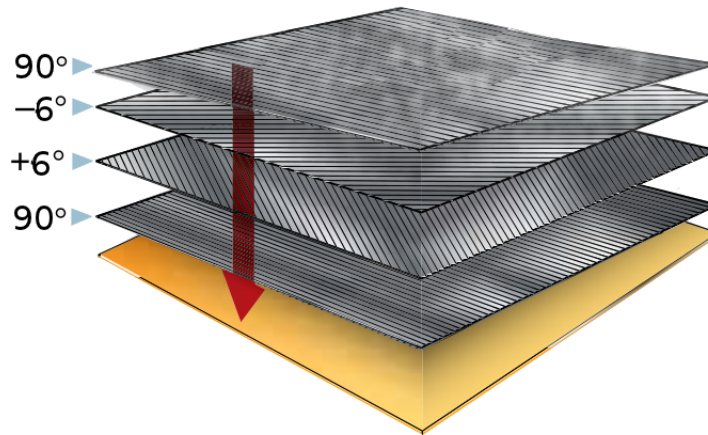


Figure 3.8: Composite layup

Winding angle on the dome changes continuously as the fibre leaves the tangent line where the dome is connected to the cylinder all the way up to the polar opening, as illustrated in Fig. 3.9.

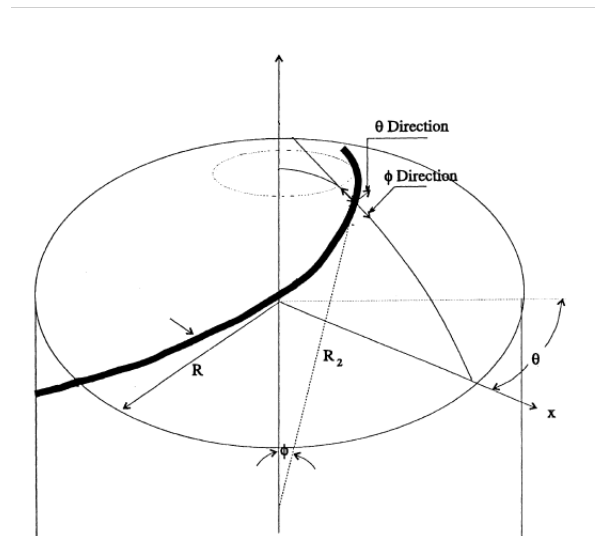


Figure 3.9: Path of the fibre

The winding angle at any point of the dome is calculated using the Clairaut's theorem (Madhavi *et al.*, 2009; Jianqiao *et al.*, 2012),

$$r \sin \alpha = \text{Constant} \quad (3.3.3)$$

where  $r$  is the radius at the point measured from the axis of the vessel and  $\alpha$  is the winding angle between the fibres and a direction of reference. In the current model the reference direction has been chosen to be the element x-axis, that is, the side joining the first to the second node, and it coincides with the  $\phi$  direction of the spherical coordinates system, as illustrated in Fig. 3.9.

Taking into consideration the fact that at the beginning of the dome the winding angle ( $\alpha$ ) is equal to the winding angle over the cylinder  $\alpha_{cyl}$ , we get

$$\begin{aligned} r \sin \alpha &= R \sin \alpha_{cyl} \\ \sin \alpha &= \frac{R}{r} \sin \alpha_{cyl} \end{aligned} \quad (3.3.4)$$

Inserting the value of  $\alpha_{cyl}$  as in Eq. E.0.1 we obtain the expression of winding angles over the domes as

$$\begin{aligned} \sin \alpha &= \frac{R_E}{r} \\ \alpha &= \sin^{-1} \left( \frac{R_E}{r} \right) \end{aligned} \quad (3.3.5)$$

where  $R_E$  is the radius measured from the axis to the centre of the winding band adjacent to the polar opening. Fig. 3.10 profiles how the winding angle changes from the aft polar opening of the vessel to its forward polar opening. The angle varies from  $90^\circ$  at the opening to  $6^\circ$  at the beginning of the cylinder. It stays constant over the cylinder and varies again at the beginning of the other dome, where it varies from  $6^\circ$  to  $90^\circ$  at the other opening.

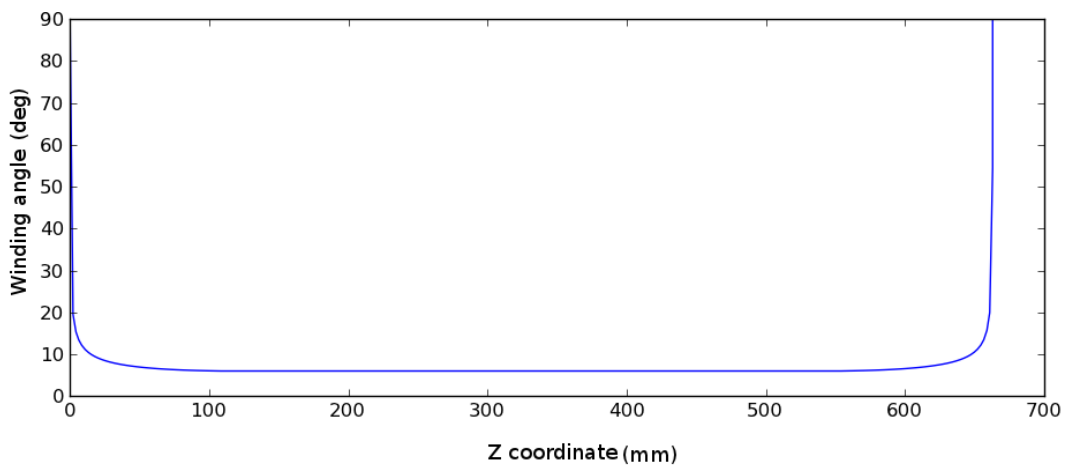


**Figure 3.10:** Change in winding angles along the axial direction

### 3.3.5 Material Properties of Elements

The composite is modelled using CQUAD4 shell elements. Element properties are defined using PCOMP composite properties. These properties are used to model layered composite. The fibres of these layers are unidirectional. They are defined by specifying each layer's composite material, its thickness and its orientation.

The composite layout depends on the winding angle which also depends on the radius, see Eq. 3.3.5. Over the cylinder, the layout is uniform but over the domes the layup is subjected to a continuous change as the radius changes continuously. To account for the change in angles, PCOMP material properties are defined using a Python script, the script sorts elements depending on the radius from the axis of the vessel at which the elements are located and assigns to those elements materials properties corresponding to the angle of the fibre at that specific radius.

### 3.3.6 Analysis

The analysis was carried out using MSC Nastran 2012 linear solution SOL 101. The solver has the ability to provide ply based results as well as element based results. In this study, we needed the value of the maximum stress in the composite. Therefore, the output of the solver was set to be the non-layered element stresses using the option of maximum stress.

### 3.3.7 Optimisation Process

The same optimisation process as in the analytical model case was followed, and DOT SQP algorithm was used again. The difference resides in the fact that the stresses were now calculated using a finite element model (FEM) for more accuracy. To replace equations with the FEM, there is need to exchange data between the optimiser and the FEM. An interfacing method between the two software has been developed using Python. At each optimisation iteration, the method reads the f06 output file of Nastran and extracts the value of the maximum stress in hoop plies, that is, plies wound at  $90^\circ$  and the maximum stress in helical plies, that is, plies wound at  $6^\circ$ . Also, the interfacing method updates values of the design variables in the bdf input file of Nastran before a new optimisation iteration starts. Results are reported in Table 3.5.

**Table 3.5:** Results of the FEM design

Parameter	Value
$t_h$ (mm)	2.95
$t_a$ (mm)	2.66
$t_{total}$ (mm)	5.61
Weight (kg)	6.63

### 3.4 Comparison of Analytical Model and Finite Element Model Results

In this section, results obtained in previous sections for the analytical and the finite element models are compared. Also, both results are compared to results of the original design of the vessel. The comparison is based on the total thickness and the total mass, as given in Table 3.6.

**Table 3.6:** Comparison of results for deterministic designs

Parameter	Original Design	Analytical Model	FEM Model
$t_{total}$ (mm)	5.6	5.8	5.6
Weight (kg)	6.61	6.52	6.63

The finite element model results are a bit lower compared to results of the analytical model, in the order of 4%, this is the result of the accuracy of stresses calculated using the finite element model. The maximum stress is found at the pole opening as shown in Fig. 3.11. The high stress at the pole opening is due to stress concentration (Jianqiao *et al.*, 2012).

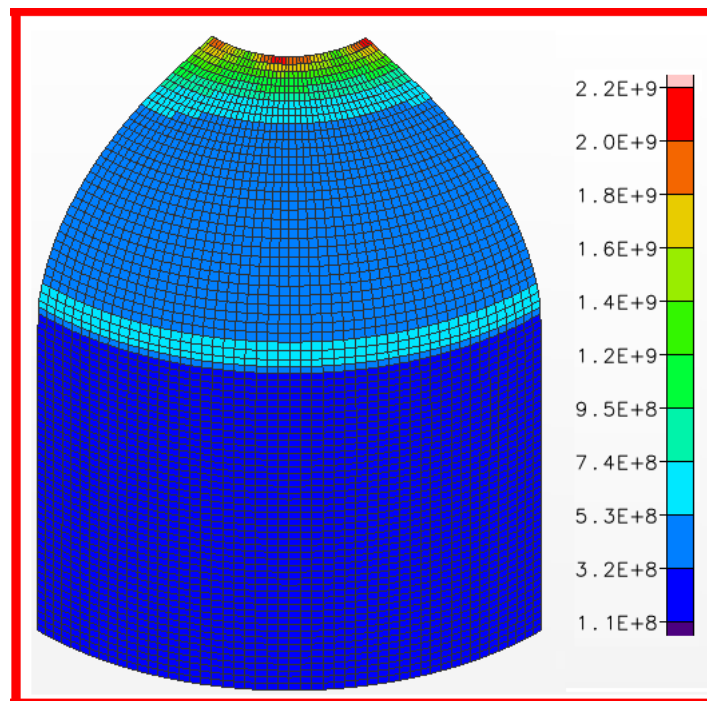


**Figure 3.11:** Von Mises stresses in the composite shell of the deterministic design

*CHAPTER 3. DETERMINISTIC DESIGN OF A COMPOSITE  
OVER-WRAPPED PRESSURE VESSEL (COPV)*

**41**

The weight estimated using Eq. D.0.20 is small compared to both the weight of the original design and the weight of the finite element model. The formula does not give the exact value of the weight, but it provides good estimates for a preliminary design.

## Chapter 4

# Reliability Based Design Optimisation (RBDO) of a Composite Over-wrapped Pressure Vessel (COPV)

In Chapter 3, the deterministic design optimisation of a COPV based on both analytical and finite element models was presented. In this chapter, an RBDO of the COPV is presented. The COPV is designed so that it can achieve the same reliability level as the deterministic design presented in Chapter 3. The aim is to show that conserving the same level of reliability, a lighter structure can be designed using reliability-based optimisation methods. First, there is a reliability analysis of the COPV using the First Order Reliability Method (FORM). The reliability obtained will then be set as the minimum allowed probability of failure of the COPV in the RBDO process as specified by Eq. 2.1.5. In the present work, Monte Carlo Simulations will be used to check results obtained using FORM.

### 4.1 Evaluation of the Probability of Failure

The reliability of the COPV is evaluated using FORM. As seen in Subsection ??, after transformation of all random variables from their original spaces to the standard normal space and the linearisation of the limit state, the evaluation of the reliability becomes an optimisation problem described by Eq. A.0.11.

To solve this optimisation problem, a Newton - Raphson type recursive method was used. The method is initialised by setting a starting point  $u_0^*$ , then recursively updating the MPP using the formula

$$\mathbf{u}_{k+1}^* = \frac{1}{|\nabla g(\mathbf{u}_k^*)|^2} [\nabla g(\mathbf{u}_k^*) \mathbf{u}_k^* - g(\mathbf{u}_k^*)] \nabla g(\mathbf{u}_k^*) \quad (4.1.1)$$

CHAPTER 4. RELIABILITY BASED DESIGN OPTIMISATION (RBDO) OF A COMPOSITE OVER-WRAPPED PRESSURE VESSEL (COPV) 43

Where  $\nabla_g(\mathbf{u}_k^*)$  is the gradient vector of the performance function at  $u_k^*$ , and the  $k^{\text{th}}$  iteration point. Note that  $k$  refers to the iteration number. Therefore,  $u_k^*$  is a vector with components  $\{u_{1k}^*, u_{2k}^*, \dots, u_{nk}^*\}$ , where  $n$  is the number of random variables.

The algorithm is repeated until at least one of the following convergence conditions is satisfied,

1.  $|\mathbf{u}_k^* - \mathbf{u}_{k-1}^*| \leq \delta$
2.  $|g(\mathbf{u}_k^*)| \leq \varepsilon$

Where  $\delta$  and  $\varepsilon$  are small quantities, say 0.001.

The recursive method is graphically represented in Fig. 4.1, where  $\mathbf{a}$  is a normalised vector of direction cosines evaluated at the design point as

$$a_i = \frac{\left(\frac{\partial g}{\partial u_i}\right)(\mathbf{u}^*)}{\sqrt{\sum_{i=1}^n \left(\left(\frac{\partial g}{\partial u_i}\right)(\mathbf{u}^*)\right)^2}} \quad (4.1.2)$$

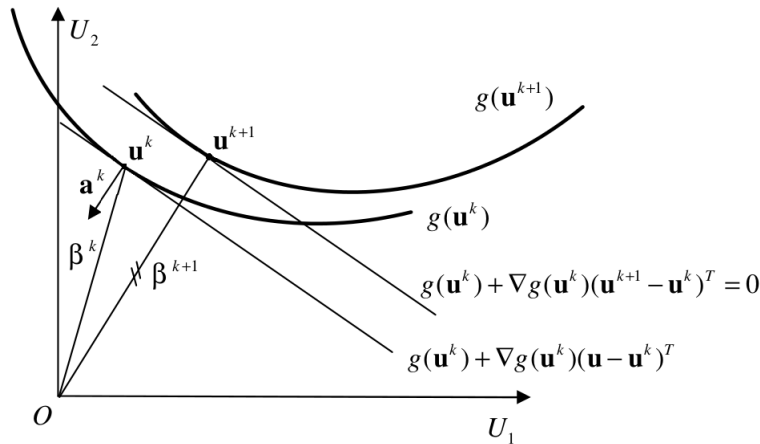


Figure 4.1: MPP recursive search method

The FORM procedure can be summarised as follows:

- I. Transform the original random variables to standard normal random variables using the Rosenblatt transformation,
- II. Solve the optimisation problem to find the MPP in the standard normal space which gives the value of the reliability index  $\beta$ .
- III. Calculate the probability of failure  $P_f = \Phi(-\beta)$



Fig. 4.2 provides a flowchart summarising the algorithm to compute the reliability index, as it has been proposed by Haldar and Mahadevan (2000), the algorithm was implemented using Python.

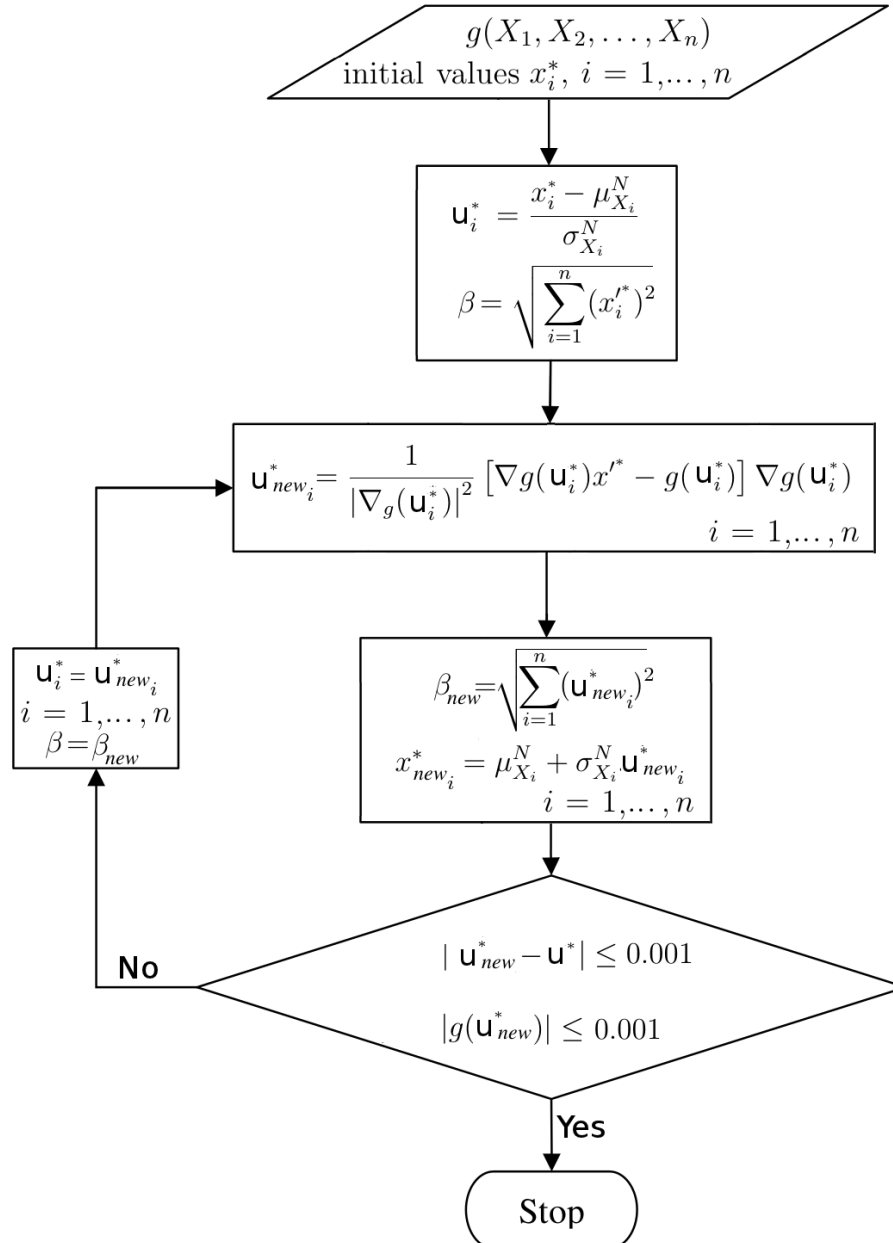


Figure 4.2: Flowchart of the FORM method.

The design of the COPV is subjected to four constraints that include two constraints that set stresses in hoop and helical plies to be less than the maximum tensile strength of the fibres, a constraint that ensures that the stress

rupture will not occur while the COPV is in service and a condition of the preferable failure region. Since any failure due to these three constraints will result in the failure of the COPV, the reliability of the COPV is calculated as a series system reliability of the three failure modes. The reliability of the system is then calculated as the union of the three failure modes. The unions in the expression of the reliability are transformed into intersections using the transformation in Eq.2.3.7. After transforming the expression, the system reliability integral given by Eq. 2.3.3 is calculated using a numerical integration method developed by Genz (1992) referred to as the Genz Algorithm. The method is described in Appendix G.

## 4.2 Analytical Model

In this section, the analytical model of a COPV based on the Classical Laminate Theory (CLT) as discussed in Chapter 3 is used in an RBDO design of a COPV. The minimum allowable probability of failure is set to be the probability of failure of the deterministic design obtained in Chapter 3. The probability of failure of the COPV is a series system probability of failure combining five failure modes, which are

- The probability of failure due the structure integrity, that is the probability that the design does not satisfy the Tsai-Wu failure criterion in hoop laminae and in helical laminae.
- The probability of failure due to strength decay in hoop and helical laminae.
- The probability of failure due the stress ratio.

The system probability of failure is evaluated using FORM alongside with the Genz algorithm. Using the probability distribution data of the design parameters defined in Table 3.2, a probability of failure of  $1.08 \times 10^{-6}$  was obtained. The accuracy of the result was checked using Monte Carlo simulation.  $10^8$  Monte Carlo experiments were used to obtain a value of  $1.05 \times 10^{-6}$ .

The probability of failure of the analytical model were then set as the minimum allowable probability of failure for the RBDO optimisation problem formulated as,

$$\begin{aligned} &\text{Minimize: Weight} \\ &\text{such that: } P_s(F) < 1.08 \times 10^{-6} \\ &10^{-3} \leq t_h, t_a \leq 10^{-2} \end{aligned} \quad (4.2.1)$$

where  $t_h$  and  $t_a$  are the hoop and the helical plies thicknesses respectively.

The values of the thicknesses obtained using the RBDO design as well as the weight of the structure are reported in Table 4.1

**Table 4.1:** Results of the analytical RBDO design

Parameter	Value
$t_h$ (mm)	2.87
$t_a$ (mm)	2.85
$t_{total}$ (mm)	5.72
Weight (kg)	6.33

Results show that a RBDO design with the same probability of failure as a deterministic design allows weight savings in the order of 3% of the weight of the deterministically designed COPV. The deterministic design takes care of stresses in hoop and helical plies only and the result is a fully stressed design with stresses that respect the stress ratio. Conversely, the RBDO design is only concerned with probabilities of failure. In the deterministic design only the Tsai-Wu failure criterion in hoop direction is critical when it comes to probability of failure. But in the RBDO design both the Tsai-Wu in hoop plies and the stress ratio failure mode are critical, as can be seen in Table 4.2.

**Table 4.2:** Individual probabilities of failure for the deterministic and the RBDO designs

Mode of failure	$P_f$ Deterministic	$P_f$ RBDO
Tsai-Wu criterion for axial layers	$1.32 \times 10^{-9}$	$1.04 \times 10^{-9}$
Tsai-Wu criterion for hoop layers	$1.8 \times 10^{-6}$	$9.68 \times 10^{-7}$
Stress rupture for axial layers	$6.2 \times 10^{-16}$	$6.2 \times 10^{-16}$
Stress rupture for hoop layers	$6.2 \times 10^{-16}$	$6.2 \times 10^{-16}$
Stress ratio condition	$3.1 \times 10^{-10}$	$1.18 \times 10^{-7}$

Where  $P_f$  stands for probability of failure.

### 4.3 Finite Element Model

In this section, the same finite element model as used in Chapter 3 was used to illustrate the design of the COPV using an RBDO method that calculates stress in the composite using a finite element model. The probability of failure of the Finite Element Model (FEM)-based deterministic design discussed in Chapter 3 was evaluated using FORM. The same procedure was used to evaluate reliability for the FEM-based RBDO. A system probability of failure of  $1.08 \times 10^{-6}$  found for the deterministic design was set as the maximum allowable probability of failure for the RBDO design.

The same optimisation problem as in the case of the analytical model was solved using the SQP algorithm of DOT. Results are summarised in Table 4.3. Results show weight savings in the order of 2% compared to those in the deterministic design while conserving the same level of reliability.

**Table 4.3:** Results of FEM based RBDO design

Parameter	Value
$t_h$ (mm)	2.84
$t_a$ (mm)	2.68
$t_{total}$ (mm)	5.52
Weight (kg)	6.48

## 4.4 Comparison of Analytical Model and FEM

In this section the comparison of results of the RBDO based on an analytical model and the RBDO based on a FEM is discussed. The thicknesses of hoop plies, the thicknesses of helical plies, the total thicknesses and the total weights from both design approaches are compared. Table 4.4 is a summary of the compared values.

**Table 4.4:** Comparison of results for RBDO design

Parameter	Analytical Model	FEM Model
$t_h$ (mm)	2.88	2.84
$t_a$ (mm)	2.83	2.68
$t_{total}$ (mm)	5.71	5.52
Weight(kg)	6.37	6.49

Again, as in the case of a deterministic design, the optimal dimensions obtained using FEM-based design are a bit smaller compared to those obtained using analytical model-based design, due to the fact that the FEM analysis stresses are more accurate, especially for the composite over the domes. Also, as in the case of the deterministic design, the weight of the analytical model estimated using Eq. D.0.20 is small compared to the weight of the finite element model. The formula underestimates the value of the weight.

## Chapter 5

# Proof Test Data Driven RBDO of a COPV

The main goal in this project is to use a real engineering example to prove that accounting for proof test data in a reliability-based design approach leads to the improvement of the original design. It is common in the design process of mechanical components that require a high level of reliability like in spacecraft, to proof test each and every designed component before they enter service. However, up to now, the use of data gathered during the proof test process has not been effectively used with the goal of improving on the design that is in place before proof testing the designed component.

In this thesis, by means of a real engineering example, we illustrated and proved the benefits of including proof test data in the design process. The design of a COPV was used in previous chapters to show that the use of RBDO methods can lead to better designs compared to the use of deterministic methods. The same example is used in this chapter to showcase that including proof test data in RBDO leads to the improvement of the RBDO design. The same analytical and FEM models as in previous chapters are used to design the vessel.

A typical design optimisation problem that accounts for proof test data is expressed by Eq. 2.4.1. In the current study, it is assumed that the component has passed the proof test successfully. The probability of passing the proof test  $P(A)$  is evaluated using FORM. The conditional probability of failure  $P(F|A)$  which is a system probability of failure given that the component has passed the proof test successfully, it is in the form of Eq. 2.5.7. Its evaluation is done using FORM together with the Genz algorithm.

The proof test of a COPV is carried out by pressurisation of the vessel at pressure higher than its operating pressure. Typically, a multiplier of 1.25 is applied to the operating pressure in order to obtain the proof pressure. However, the method used in this study provides the designer with the ability to control the magnitude of the proof test loads by setting a probability of success of the proof test.

The choice of the probability of successfully passing the proof test is a trade-off between achieving higher levels of reliability, and allowing improvement of the design. For the current project design, improvement is evaluated in terms of weight savings. In cases where the cost of failing the proof test is bearable, the designer can choose to set higher probabilities of failing the proof test and achieve significant weight savings. In contrast, if failing the proof test is costly, the designer might choose to set higher probability of passing the proof test and achieve moderate weight savings.

The allowable probability of failure of the system given that it has passed the proof test successfully  $P_{req}$  is set to be equal to the probability of failure of the deterministic design,  $P_{req} = 1.08 \times 10^{-6}$ . The optimisation problem is then formulated as

$$\begin{aligned}
 &\text{Minimize: Weight} \\
 &\text{such that: } P(F|A) \leq 1.08 \times 10^{-6} \\
 &\quad 1 - P(A) \leq P_{proof} \\
 &\quad 10^{-3} \leq \tau_{hoop}, \tau_{helical} \leq 10^{-2} \\
 &\quad 3.1 \times 10^6 \leq p_p \leq 4.65 \times 10^6
 \end{aligned} \tag{5.0.1}$$

where  $P_s(F|A)$  is the conditional probability of failure of the system given that it has been passed the proof test successfully.  $1 - P(A)$  is the probability of failing the proof test. The last two constraints set the upper and lower limits of the thicknesses and the proof pressure. Thicknesses are constrained to be between 1 mm and 5 mm and the proof test magnitude cannot be lower than the operational pressure or higher than the burst pressure, which is estimated to be 1.5 times the operational pressure.

As seen in Eq. 5.0.1, the magnitude of the proof test load  $p_p$  is part of the design variables. That equips the designer with the ability to design the proof test level by setting the probability of failing the proof test depending on the the level of reliability he wants to achieve. In this study the optimisation is done for different values of  $P_{proof}$  ranging from 0% to 0.1%. A trade-off graph representing the variation of the proof pressure when the probability of failing the proof test is varied, is presented in Fig. 5.1.

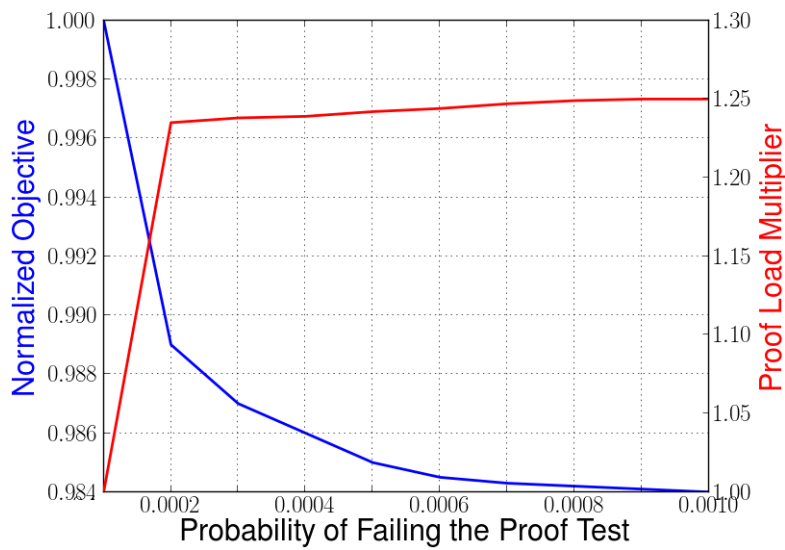


**Figure 5.1:** Trade-off graph between the proof test magnitude and the probability of failing the proof test.

From Fig.5.1 it can be seen that including the proof test in the RBDO design process allows for further weight savings while preserving the reliability level as the deterministic design. In the present particular case, weight savings of about 1.5% compared to those of the RBDO design without proof test can be made, if a probability of failing the proof test of 1 in 1000 is allowed.

# Chapter 6

## Conclusions

The work presented in this thesis was concerned with the application of Reliability-Based Design Optimisation (RBDO) method that includes proof test data in the design process. The method was applied to the design of a Composite Over-wrapped Pressure Vessel (COPV). The main goal was to prove that considering proof test data in the design process can allow the designer to improve on the original design used for the proof tested component.

Features of the design method presented in this thesis have been implemented and applied to the design of a COPV. The design of a COPV was concerned with minimisation of the weight. The method was proven to be advantageous compared to standard RBDO and deterministic methods in terms of weight savings. Moreover, it was shown that the method enables the designer to set the magnitude of the proof test load, based on the choice of a probability of failing the proof test.

### 6.1 Overview

In the first stage of the project, a review of design tools commonly used in industry was presented. Two design methods were of interest.

- Deterministic design optimisation
- Reliability Based Design Optimisation (RBDO).

These two design methods were assessed and set as the basis of comparison for the method studied in this project.

For both design methods, optimisation was carried out using the Sequential Quadratic Programming (SQP) algorithm of the Vanderplaats design optimisation tools (DOT) suite. Particularly, for RBDO methods, reliability was evaluated using the First Order Reliability Method (FORM). FORM was implemented using Python based on a Newton-Raphson algorithm that searches for the Most Probable Point (MPP)



The optimisation of the design of a COPV was concerned with weight minimisation. The Tsai-Wu failure criterion was used to ensure the structural integrity of the design, and the vessel was designed to last more than twenty years in service by modelling the stress rupture failure using the strength decay model. The COPV was modelled using both its analytical model based on the classic laminate theory and its finite element model developed using MSC Patran as pre- and post-processor and MSC Nastran as a solver.

Results showed that for the same level of reliability, including proof test data in RBDO allows significant weight savings compared to standard RBDO and deterministic design methods. It was also shown that the level of proof test has an influence on the design, and the designer has control over it. Depending on the cost that will involve the failure of a proof test, the designer can choose to set high probability of failing the proof test and have significant weight savings, or set low probability of failing the proof test and get minor weight savings.

## 6.2 Future Work

The application of the RBDO that accounts for proof test data as presented in this thesis has proven the effectiveness of the method. However, the implementation of the method can be improved in a number of ways to make it more effective and flexible. The following are some of the improvements that can be made to the implementation of the method,

- The use of reliability methods other than FORM. In this study, FORM was chosen for reliability estimation. However, depending on the problem being studied, other reliability methods such as the Second Order Reliability Method (SORM) can give better reliability estimations. Therefore, the consideration of other reliability methods can improve on the accuracy of reliability estimation in RBDO.
- The use of non normal correlated random variables. In the current implementation of the method, all random variables are assumed to be uncorrelated and normally distributed. In real engineering problems, parameters are often correlated and follow various probability distributions. The consideration of correlated non normal random variables will expand the method and make its application to a wide range of engineering problems easier.
- Considering the case where the proof test is not passed successfully. In this study, the influence of a successful proof test on the design process has been assessed. However, it might be of interest to assess the influence of a failed proof test on the design process.
- Use of non gradient based optimisers. The sequential quadratic programming method used in this study depends on the starting point,

and in some cases the optimisation process leads to a local minimum. The consideration of population based optimisation algorithms such as the Particle Swarm Optimisation (PSO) or the Genetic Algorithm (GA) would lead to a better global optimisation. Also, in some cases, discrete optimisation algorithms are more appropriate. As an example, the use of integer programming for the optimisation of the COPV would have allowed to optimise not only the thickness of the composite overwrap, but also the number of plies.

# Appendices

# Appendix A

## The First Order Reliability Method (FORM)

FORM is an analytical approximation method used to approximate the probability integral

$$P_f = \int \dots \int_{g(X_1, X_2, \dots, X_n) \leq 0} f(X_1, X_2, \dots, X_n) dX_1 dX_2 \dots dX_n \quad (\text{A.0.1})$$

Where  $f(X_1, X_2, \dots, X_n)$  is the joint probability density function for the basic random variables  $X_1, X_2, \dots, X_n$  and  $g(X_1, \dots, X_n)$  the limit state function.

In FORM the limit state function  $g(X_1, \dots, X_n)$  is linearised by approximating it using the first order Taylor expansion. FORM simplifies the probability integration using a two-step procedure. The first step involves the simplification of the function  $f(X_1, \dots, X_n)$  so that its contours become more regular and symmetric, and the second step is the linearisation of the integration boundary  $g(X_1, \dots, X_n) = 0$ .

The simplification of the integrand is achieved by the transformation of all basic variables from their original space referred to as  $X$ , to a standard normal space referred to as  $U$ . In the new space all the random variables  $U_1, \dots, U_n$  follow the standard normal distribution. The transformation from  $X$  to  $U$  is based on the condition that the cumulative distribution functions of the random variables remain the same in both spaces. This type of transformation is called the Rosenblatt transformation (Rosenblatt, 1952), which is expressed by

$$F_{X_i}(X_i) = \Phi(U_i) \quad (\text{A.0.2})$$

The transformed standard normal variable is then given by

$$U_i = \Phi^{-1} [F_{X_i}(X_i)] \quad (\text{A.0.3})$$

For example, a normally distributed random variable  $X$  with mean  $\mu$  and standard deviation  $\sigma$ ,  $X=N(\mu, \sigma)$  is transformed into

$$U = \Phi^{-1} [F_X(X)] = \Phi^{-1} \left[ \Phi \left( \frac{X - \mu}{\sigma} \right) \right] = \frac{X - \mu}{\sigma} \quad (\text{A.0.4})$$

Correlated non-normal random variables are first transformed into normal uncorrelated random variables using appropriate transformations (Haldar and Mahadevan, 2000) before transformation into normal standard random variables.

After the transformation, the limit state function  $g(X_1, \dots, X_n)$  will change to  $g(U_1, \dots, U_n)$  denoting the transformed limit state function in the standard space, and the fundamental equation of reliability analysis becomes

$$P_f = \int \dots \int_{g(U) \leq 0} f(U_1, U_2, \dots, U_n) dU_1 dU_2 \dots dU_n \quad (\text{A.0.5})$$

The transformed probability integrations in the reduced normal space is visualised with a two-dimensional case in Fig. A.1. Note that, after the transformation the contours are regular and circular.

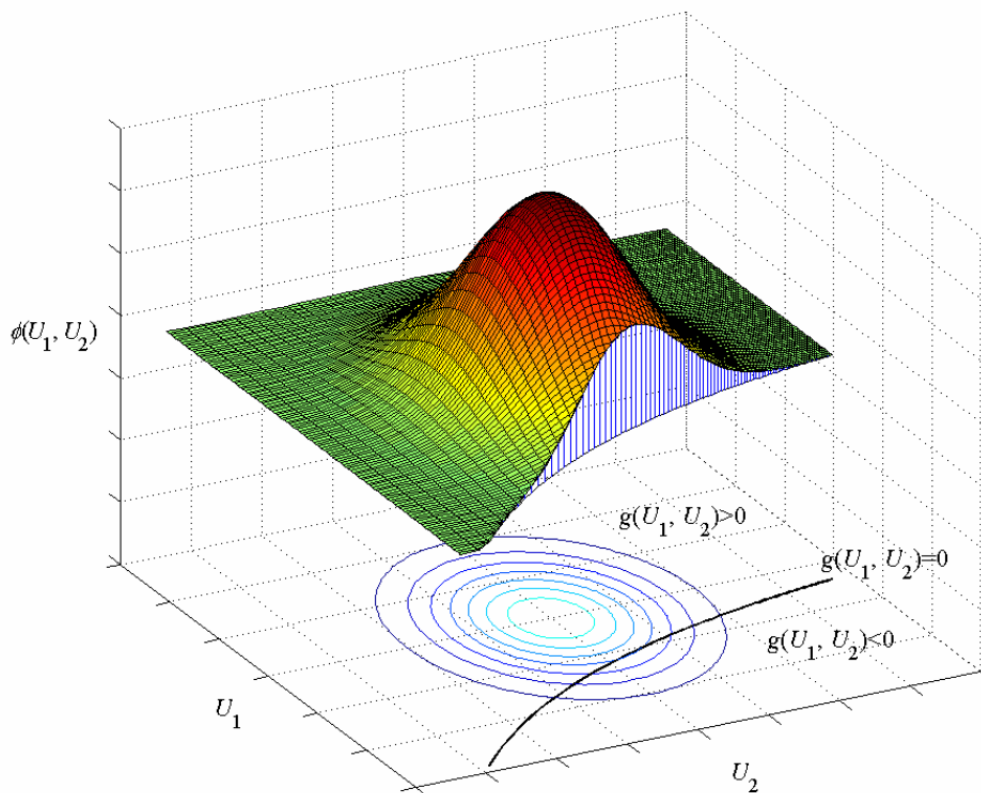


**Figure A.1:** Probability integration surface in reduced standard normal space (Du, 2005).

Since all random variables are independent standard normal random variables, the joint probability density can be expressed as the product of the individual probability densities (Haldar and Mahadevan, 2000) and it is then

given by

$$f(U_1, U_2, \dots, U_n) = \prod_{i=1}^n \frac{1}{\sqrt{2\pi}} \exp\left(-\frac{1}{2}U_i^2\right) \quad (\text{A.0.6})$$

and the probability integration becomes

$$P_f = \int \dots \int_{g(\mathbf{U}) \leq 0} \prod_{i=1}^n \frac{1}{\sqrt{2\pi}} \exp\left(-\frac{1}{2}U_i^2\right) dU_1 dU_2 \dots dU_n \quad (\text{A.0.7})$$

Furthermore, the probability integration is simplified even more in FORM by the use of a linear approximation of the limit state function using its first order Taylor series expression

$$g(\mathbf{U}) = g(\mathbf{U}^*) + \nabla g(\mathbf{U}^*)(\mathbf{U} - \mathbf{U}^*)^T \quad (\text{A.0.8})$$

where  $\mathbf{U}^* = (U_1^*, \dots, U_n^*)$  is the expansion point and  $\nabla g(\mathbf{U}^*)$  the gradient of  $g(\mathbf{U})$  at  $\mathbf{U}^*$  given by

$$\nabla g(\mathbf{U}^*) = \left( \frac{\partial g(\mathbf{U})}{\partial U_1}, \frac{\partial g(\mathbf{U})}{\partial U_2}, \dots, \frac{\partial g(\mathbf{U})}{\partial U_n} \right) \Big|_{\mathbf{U}^*} \quad (\text{A.0.9})$$

For an accurate approximation, the performance function has to be expanded at a point that has the highest contribution to the probability integration. That is, a point located on the limit state function that has the highest probability density, referred to as the Most Probable Point (MPP). The mathematical model to locate the MPP is

$$\begin{aligned} \text{Maximize: } & \prod_{i=1}^n \frac{1}{\sqrt{2\pi}} \exp\left(-\frac{1}{2}U_i^2\right) \\ \text{such that: } & g(\mathbf{U}) \leq 0 \end{aligned} \quad (\text{A.0.10})$$

Since maximising  $\prod_{i=1}^n \frac{1}{\sqrt{2\pi}} \exp\left(-\frac{1}{2}U_i^2\right)$  is equivalent to minimising  $\sum_{i=1}^n U_i^2$ , the problem becomes the minimisation of the norm of the vector  $\mathbf{U}$  given by

$$\begin{aligned} \text{Minimize: } & \|\mathbf{U}\| = \sqrt{\sum_{i=1}^n U_i^2} \\ \text{such that: } & g(\mathbf{U}) \leq 0 \end{aligned} \quad (\text{A.0.11})$$

Then, the MPP is a point on the limit state that is closest to the origin in the standard normal space, as shown in Fig. A.2.

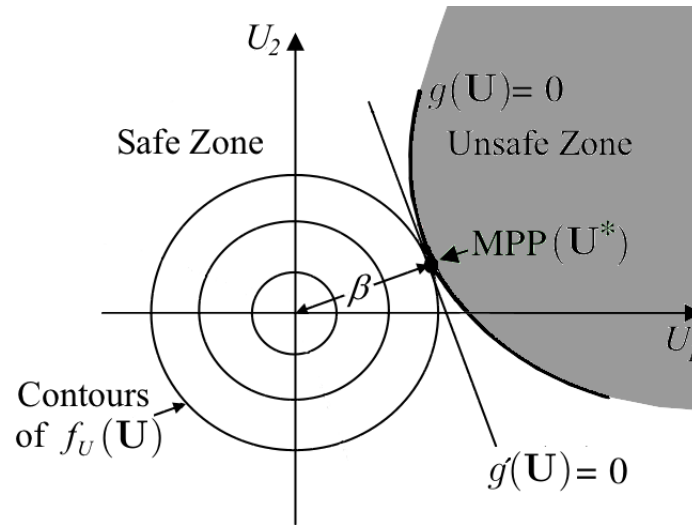


Figure A.2: Most probable point

## Appendix B

# The Second Order Reliability Method (SORM)

The second order reliability method (SORM) is an analytical method that approximates reliability using the second order Taylor expansion of the limit state function,

$$g(\mathbf{U}) = g(\mathbf{U}^*) + \nabla g(\mathbf{U}^*)(\mathbf{U} - \mathbf{U}^*)^T + \frac{1}{2}(\mathbf{U} - \mathbf{U}^*)\mathbf{H}(\mathbf{U}^*)(\mathbf{U} - \mathbf{U}^*)^T \quad (\text{B.0.1})$$

where  $\mathbf{H}(\mathbf{U}^*)$  is the Hessian matrix evaluated at the design point

$$\mathbf{H}(\mathbf{U}^*) = \begin{bmatrix} \frac{\partial^2 g(\mathbf{U})}{\partial U_1^2} & \frac{\partial^2 g(\mathbf{U})}{\partial U_1 \partial U_2} & \cdots & \frac{\partial^2 g(\mathbf{U})}{\partial U_1 \partial U_n} \\ \frac{\partial^2 g(\mathbf{U})}{\partial U_2 \partial U_1} & \frac{\partial^2 g(\mathbf{U})}{\partial U_2^2} & \cdots & \frac{\partial^2 g(\mathbf{U})}{\partial U_2 \partial U_n} \\ \cdots & \cdots & \cdots & \cdots \\ \frac{\partial^2 g(\mathbf{U})}{\partial U_n \partial U_1} & \frac{\partial^2 g(\mathbf{U})}{\partial U_n \partial U_2} & \cdots & \frac{\partial^2 g(\mathbf{U})}{\partial U_n^2} \end{bmatrix}_{\mathbf{U}=\mathbf{U}^*} \quad (\text{B.0.2})$$

In SORM, the limit state is further simplified rotating the coordinate system by an angle  $\theta$  such that the last variable  $U_n$  coincides with the direction cosine vector  $\mathbf{a}$  oriented from the origin to the design point. Fig. B.1 illustrates the rotation of the coordinate system for a simple example of two variables.



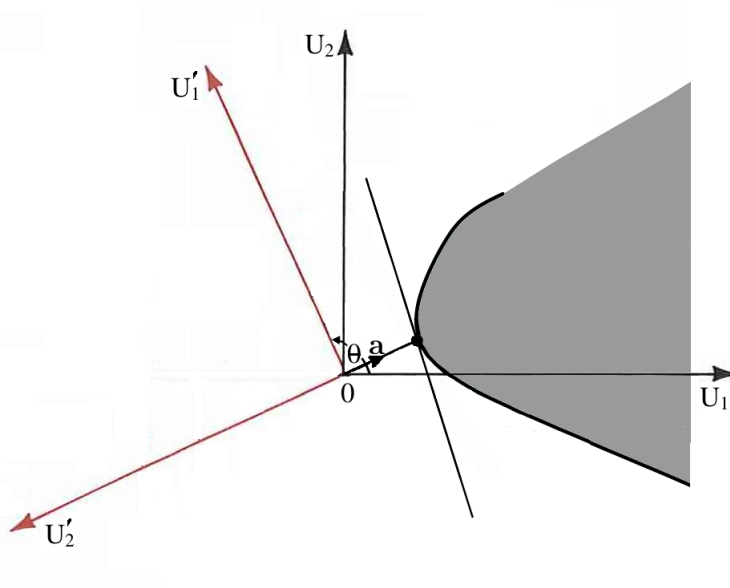


**Figure B.1:** Rotation of coordinates

The rotation transforms the space  $U$  into a new rotated space  $U'$  through the transformation

$$\mathbf{U}' = \mathbf{R}\mathbf{U} \quad (\text{B.0.3})$$

The rotation matrix  $\mathbf{R}$  is obtained using Gram-Schmidt orthogonalisation of the matrix

$$\mathbf{R}_0 = \begin{bmatrix} 1 & 0 & \dots & 0 \\ 0 & 1 & \dots & 0 \\ \dots & \dots & \dots & \dots \\ 0 & 0 & \dots & 1 \\ a_1 & a_2 & \dots & a_n \end{bmatrix} \quad (\text{B.0.4})$$

where  $a_1, a_2, \dots, a_n$  are the components of the direction cosine vector  $\mathbf{a}$ . In the new space the limit state function can be rewritten as

$$g(\mathbf{U}') = U'_n - \left( \beta + \frac{1}{2} \mathbf{U}'^T \mathbf{A} \mathbf{U}' \right) \quad (\text{B.0.5})$$

where  $\mathbf{A}$  is an  $(n-1) \times (n-1)$  matrix of which the elements are

$$a_{ij} = \frac{(\mathbf{R}\mathbf{H}\mathbf{R}^T)_{ij}}{|\nabla g(\mathbf{U}^*)|}, \quad i, j = 1, 2, \dots, n-1 \quad (\text{B.0.6})$$

where  $\mathbf{R}$  is the rotation matrix,  $\mathbf{H}$  is the Hessian matrix evaluated at the design point in the normal standard space and  $|\nabla g(\mathbf{u}^*)|$  is the norm of the gradient vector evaluated at the design point in the normal standard space. Note that in this expression the last variable  $U'_n$  is not considered because it coincides with the vector  $\beta$  evaluated using the First Order Reliability Method (FORM)

discussed in Appendix A. An approximation of the probability of failure is then calculated using the theory of asymptotic approximations (Breitung, 1984) as

$$P_f = \Phi(-\beta) \prod_{i=1}^{n-1} (1 + \beta \kappa_i)^{-1/2} \quad (\text{B.0.7})$$

where  $\kappa_i$  are the principal curvatures of the limit state at the MPP. The principal curvatures are calculated as eigenvalues of the matrix  $\mathbf{A}$ .

Generally SORM is more accurate than FORM since it takes into consideration the curvature of the limit state as illustrated in Fig. B.2. However, SORM is not computationally efficient since it requires the evaluation of the second order derivatives, hence involving a large number of function evaluations. Also, the probability of failure in SORM is determined using the theory of asymptotic approximation which is accurate only when  $\beta$  is large, as small values of  $\beta$ , SORM can be inaccurate (Haldar and Mahadevan, 2000).

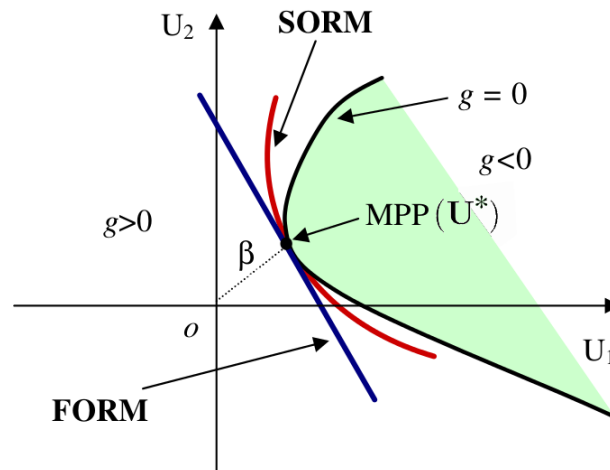


**Figure B.2:** Comparison of FORM and SORM

# Appendix C

## Finite Difference Method

The finite difference method is based on the definition of partial derivatives,

$$\frac{\partial g(\mathbf{x})}{\partial x_i} = \lim_{\Delta x_i \rightarrow 0} \frac{\Delta g(x_1^*, x_2^*, \dots, x_i^* + \Delta x_i, \dots, x_n^*)}{\Delta x_i} \quad (\text{C.0.1})$$

Where  $x^* = x_1^*, x_2^*, \dots, x_n^*$  is the point at which the derivative is evaluated and  $\Delta x_i$  a small variation of the variable  $x_i$ . It turns out that for small values of perturbations in variables, the ratio of the change in the limit state to the perturbation is a good approximation of the derivative of the limit state with respect to the perturbed variable at a given point. Therefore, the finite difference method can be used to calculate the derivatives at the MPP required in FORM and SORM. An algorithm to compute partial derivatives at the MPP  $x^* = x_1^*, x_2^*, \dots, x_n^*$  can be described as

1. Compute  $Z_0 = g(x_1^*, x_2^*, \dots, x_n^*)$
2. Change the value of  $x_1^*$  to  $(x_1^* + \Delta x_1)$ , where  $\Delta x_1$  is a small variation, say 0.001, referred to as perturbation in the value of  $x_1$ , all the other variables keeping their original values, and compute  $Z_1 = g(x_1^* + \Delta x_1, x_2^*, \dots, x_n^*)$ .
3.  $\frac{\Delta Z}{\Delta x_1} = \frac{Z_1 - Z_0}{\Delta x_1}$  approximates the derivative of  $g(\mathbf{x})$  with respect to  $x_1$ .
4. Repeat steps 2 and 3 for each variable.

## Appendix D

# Calculation of the Composite Overwrap Thickness and Weight

The thickness of the composite can be calculated using analytical methods such as the netting analysis (Peters *et al.*, 2011) or the Classical Laminate Theory (CLT) (Daniel and Ishai, 2006). In this thesis, the CLT method is used.

The CLT considers only thicknesses of fibre plies on the cylindrical part of the COPV, stresses in the domes are not accounted for directly. To account for stresses in the domes, a design factor known as the stress ratio is used. The stress ratio is defined as the ratio of the allowable stress in the helical windings to the allowable stress in the hoop windings. The stress ratio provides the designer with the ability to define which failure mode prevails. For ratios lower than 90%, the hoop failure mode prevails, and for 100% and greater, the helical failure prevails.

It is preferred to have a hoop failure because hoop failures are predominantly affected by internal pressure that makes them accurately predictable. Helical failures are strongly affected by the bending loads, and that makes them complex and hard to predict. Mixed-mode failures (stress ratios between 90% and 100%) are also not recommended due to their complexity. It is therefore recommended that a stress ratio between 60% and 85% be set (Peters *et al.*, 2011).

The stress ratio increases the thickness of the composite in the dome regions to account for complex unknown stresses in that region. This approach is inaccurate and can result in either over designed or under designed composite plies in the dome region. For a better analysis of stresses in the dome region that considers the shape of the dome, multiple wind angle and the resin contribution, a finite element analysis is preferred.

In CLT, a laminate is considered as an organised stack of plies each of which is composed of fibres oriented in a single direction. The laminate is defined by specifying the directions of its constituent plies. As an examples [90, -6, 6, 90] represents a laminate composed of 4 plies with fibres oriented in directions specified by the angles in brackets. The CLT describes elastic properties of

laminated composites with the following assumptions,

- Laminae are perfectly bonded,
- Bond between laminae are infinitesimally thin,
- Straight lines normal to the middle surface remain straight,
- Strain perpendicular to the middle surface is ignored.

The middle surface is then selected as a reference plane.

In CLT, two type of coordinate systems are considered, a global coordinate system that often coincides with the loading of the laminate and is referred to as the  $(x, y, s)$  coordinate system where  $s$  refers to the shear in the  $(x, y)$  plane, and laminae coordinate systems referred to as  $(1, 2, 6)$  coordinate systems where 6 refers to the shear in the  $(1, 2)$  plane. The strain at any point in the laminated composite is then given by the relation,

$$\begin{bmatrix} \varepsilon_x \\ \varepsilon_y \\ \gamma_s \end{bmatrix} = \begin{bmatrix} \varepsilon_x^0 \\ \varepsilon_y^0 \\ \gamma_s^0 \end{bmatrix} + z \begin{bmatrix} \kappa_x \\ \kappa_y \\ \kappa_s \end{bmatrix} \quad (\text{D.0.1})$$

where  $\varepsilon_x^0, \varepsilon_y^0, \gamma_s^0$  are the mid-surface strains and  $\kappa_x, \kappa_y, \kappa_s$  are the curvatures and  $z$  is the distance from the mid surface to the point where the strain is measured.

Each lamina compliance matrix is given by the equation

$$\mathbf{S} = \begin{bmatrix} \frac{1}{E_1} & -\frac{\nu_{21}}{E_2} & 0 \\ -\frac{\nu_{21}}{E_2} & \frac{1}{E_2} & 0 \\ 0 & 0 & \frac{1}{G_{12}} \end{bmatrix} \quad (\text{D.0.2})$$

where  $E_1$  and  $E_2$  are respectively the Young's moduli in the axial and transverse directions of the fibres and  $G_{12}$  the shear modulus.

$$\nu_{21} = \nu_{12} \times \frac{E_1}{E_2} \quad (\text{D.0.3})$$

where  $\nu_{12}$  is the Poison's ratio. Each lamina modulus matrix  $\mathbf{Q}$  is then obtained as the inverse of its compliance matrix. That is,

$$\mathbf{Q} = \mathbf{S}^{-1} \quad (\text{D.0.4})$$

Laminae in a composite are oriented in different directions. In order to calculate the strain in the global coordinate system, laminae are rotated using the transformation

$$\mathbf{T} = \begin{bmatrix} \cos^2 \theta & \sin^2 \theta & 2 \sin \theta \cos \theta \\ \sin^2 \theta & \cos^2 \theta & -2 \sin \theta \cos \theta \\ -\sin \theta \cos \theta & \sin \theta \cos \theta & \cos^2 \theta - \sin^2 \theta \end{bmatrix} \quad (\text{D.0.5})$$

where  $\theta$  is the orientation of the fibres in the lamina, that is, the angle between the axial direction of the fibres and the  $X$ -axis of the global coordinate system. The lamina global modulus matrix is then calculated as

$$\mathbf{Q}_{xys} = \mathbf{TQT}^{-1} \quad (\text{D.0.6})$$

Forces and moments acting on the laminate are directly related to the stress and deformation in each lamina. Considering the strain in each lamina and using the relation (D.0.1), force resultants can be written as

$$\begin{aligned} \mathbf{N} &= \sum_{k=1}^n \left( \int_{z_{k-1}}^{z_k} (\mathbf{Q}_{xys}^k \boldsymbol{\varepsilon}^0 + z \mathbf{Q}_{xys}^k \boldsymbol{\kappa}) dz \right) \\ \mathbf{N} &= \sum_{k=1}^n \left( \mathbf{Q}_{xys}^k \boldsymbol{\varepsilon}^0 \int_{z_{k-1}}^{z_k} dz + \mathbf{Q}_{xys}^k \boldsymbol{\kappa} \int_{z_{k-1}}^{z_k} z dz \right) \\ \mathbf{N} &= \left( \sum_{k=1}^n \mathbf{Q}_{xys}^k (z_k - z_{k-1}) \right) \boldsymbol{\varepsilon}^0 + \left( \frac{1}{2} \sum_{k=1}^n \mathbf{Q}_{xys}^k (z_k^2 - z_{k-1}^2) \right) \boldsymbol{\kappa} \end{aligned} \quad (\text{D.0.7})$$

This can be rewritten in a matrix form as

$$\begin{bmatrix} N_x \\ N_y \\ N_z \end{bmatrix} = \begin{bmatrix} A_{11} & A_{12} & A_{16} \\ & A_{22} & A_{26} \\ Sym & & A_{66} \end{bmatrix} \begin{bmatrix} \varepsilon_x^0 \\ \varepsilon_y^0 \\ \gamma_s^0 \end{bmatrix} + \begin{bmatrix} B_{11} & B_{12} & B_{16} \\ & B_{22} & B_{26} \\ Sym & & B_{66} \end{bmatrix} \begin{bmatrix} \kappa_x \\ \kappa_y \\ \kappa_s \end{bmatrix} \quad (\text{D.0.8})$$

where  $\mathbf{A}$  is a symmetric matrix referred to as the laminate extensional stiffness matrix or the in-plane moduli matrix defined as

$$A_{ij} = \sum_{k=1}^n Q_{ij}^k (z_k - z_{k-1}) \quad (\text{D.0.9})$$

$\mathbf{B}$  is also a symmetric matrix referred to as the laminate coupling matrix defined as

$$B_{ij} = \frac{1}{2} \sum_{k=1}^n Q_{ij}^k (z_k^2 - z_{k-1}^2) \quad (\text{D.0.10})$$

$z_k$  is the distance from the mid-surface to the layer  $k$ . Similarly, moment resultants are obtained as

$$\begin{bmatrix} M_x \\ M_y \\ M_z \end{bmatrix} = \begin{bmatrix} B_{11} & B_{12} & B_{16} \\ & B_{22} & B_{26} \\ Sym & & B_{66} \end{bmatrix} \begin{bmatrix} \varepsilon_x^0 \\ \varepsilon_y^0 \\ \gamma_s^0 \end{bmatrix} + \begin{bmatrix} D_{11} & C_{12} & D_{16} \\ & C_{22} & D_{26} \\ Sym & & D_{66} \end{bmatrix} \begin{bmatrix} \kappa_x \\ \kappa_y \\ \kappa_s \end{bmatrix} \quad (\text{D.0.11})$$

where  $\mathbf{D}$  is the laminate bending stiffness matrix given by

$$D_{ij} = \frac{1}{3} \sum_{k=1}^n Q_{ij}^k (z_k^3 - z_{k-1}^3) \quad (\text{D.0.12})$$

The load-deformation relations in global coordinates is then calculated as

$$\begin{bmatrix} \boldsymbol{\varepsilon}_{xys}^0 \\ \boldsymbol{\kappa}_{xys}^0 \end{bmatrix} = \begin{bmatrix} \mathbf{A} & \mathbf{B} \\ \mathbf{B} & \mathbf{D} \end{bmatrix}^{-1} \begin{bmatrix} \mathbf{N} \\ \mathbf{M} \end{bmatrix} \quad (\text{D.0.13})$$

where  $\boldsymbol{\varepsilon}_{xys}^0$  and  $\boldsymbol{\kappa}_{xys}^0$  are respectively the mid-surface strains and curvatures. Using Eq. D.0.1 the strain at any point of the laminate can be obtained. The stress in a given layer of the composite is then calculated as

$$\boldsymbol{\sigma}_{xys} = \bar{\mathbf{Q}}_{xys} \boldsymbol{\varepsilon}_{xys} \quad (\text{D.0.14})$$

Where  $\bar{\mathbf{Q}}$  is the reduced lamina global matrix defined as

$$\bar{\mathbf{Q}}_{xys} = \mathbf{T}^{-1} \mathbf{Q} \mathbf{B} \mathbf{T} \mathbf{B}^{-1} \quad (\text{D.0.15})$$

Where  $\mathbf{B}$  is the Reuter's matrix defined by

$$\mathbf{B} = \begin{bmatrix} 1 & 0 & 0 \\ 0 & 1 & 0 \\ 0 & 0 & 2 \end{bmatrix} \quad (\text{D.0.16})$$

COPVs are preferred over homogeneous metallic pressure vessels due to their high strength to weight ratio. In most applications, COPVs are used for the storage of fuel in space craft where any weight savings can increase the payload of the vehicle. For that reason, the optimisation of a COPV design is mostly a minimisation of its weight. For this purpose, it is necessary to establish a performance function that expresses the total weight of the vessel.

In the case of the cylindrical part of the vessel, the weight can easily be calculated using the formula

$$W_{cyl} = 2\pi R L_{cyl} \rho t_{cyl} \quad (\text{D.0.17})$$

where  $W_{cyl}$  is the cylinder weight,  $L_{cyl}$  the cylinder length,  $R$  the cylinder inner radius and  $\rho$  the density of the composite.

In the case of domes, the calculation of the weight is not straightforward, and it involves the use of numerical integration. A simplified equation (Peters *et al.*, 2011) that gives a close estimation of the weight of the composite overwrap in the dome region is

$$W_{Dome} = c R^2 \rho t_a \quad (\text{D.0.18})$$

where  $c$  is a constant determined using the nomogram in Fig. D.1, where  $R_E$  is the radius measured from the axis to the centre of the winding band adjacent to the polar opening and  $R$  the inner radius of the cylinder.

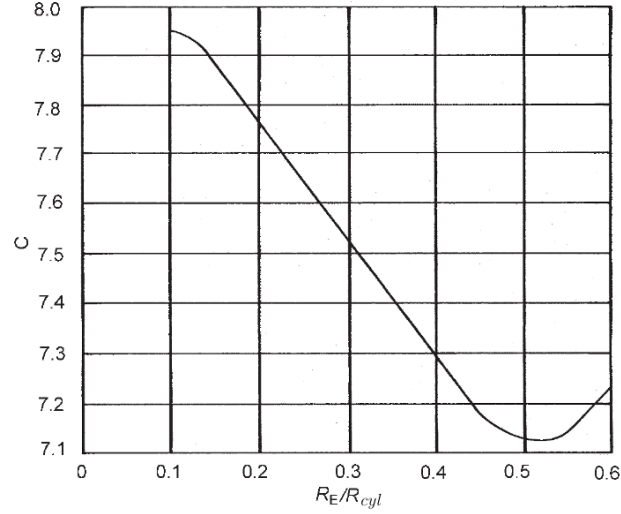


**Figure D.1:** Nomogram for the estimation of the weight of geodesic domes (Peters *et al.*, 2011)

The total weight of the pressure vessel is defined as the sum of Eq. D.0.17 and Eq. D.0.18 resulting in the equation:

$$W_{Tot} = 2\pi RL_{cyl}\rho(t_h + t_a) + 2cR^2\rho t_a \quad (D.0.19)$$

Since dividing an equation by a constant doesn't affect its minimum, the performance function can be rewritten as

$$f(t_h, t_a) = \pi L_{cyl}(t_h + t_a) + cRt_a \quad (D.0.20)$$

The parameter  $c$  is read from the nomogram presented in Fig. D.1. To read the value of  $c$ , we need to calculate the value of  $R_E/R$  where  $R_E$  is the radius measured from the axis of the vessel to the centre of the winding band adjacent to the polar opening and  $R$ , the inner radius of the cylinder. Typically, the band widths are between 2 and 4% of the vessel diameter (Peters *et al.*, 2011). In this study, we consider the band width to be 3% of the diameter and we take the radius of the opening to be the average of the radii of both openings. Results for the value of  $c$  are given in Table D.1.

**Table D.1:** Value of the parameter  $c$

Parameter	Value
$R_E$	21.63 mm
$R_E/R$	0.1
$c$	7.95



## Appendix E

# Determination of the Winding Angle

The composite overwrap is wound in two directions, the hoop direction and the longitudinal direction. Hoop windings cover the cylinder and resist pressure in the radial direction. Longitudinal windings cover both the cylinder and the domes. They mostly resist pressure in the axial direction. Fibres in the longitudinal direction are helically wound at an angle defined by using a semi empirical formula established based on experience, the formula is defined depending on the shape of the dome, the radius of the cylinder and the radius of the opening (Peters *et al.*, 2011). For geodesic domes, the winding angle

$$\alpha = \sin^{-1} \left( \frac{R_E}{R} \right) \quad (\text{E.0.1})$$

Where  $R_E$  is the radius to the centre of the winding band, and  $R$  is the radius of the vessel.

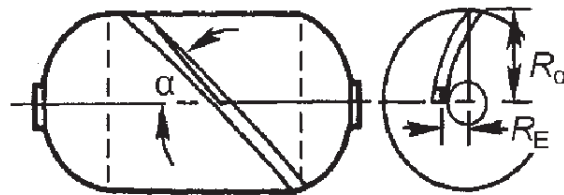


**Figure E.1:** Winding angle for geodesic domes (Peters *et al.*, 2011)

Eq. E.0.1 is valid when the diameters of both openings are the same. In the case of two domes with different diameters, the winding angle is

$$\alpha = \frac{\alpha_{FWD} + \alpha_{AFT}}{2} \quad (\text{E.0.2})$$

where  $\alpha_{FWD}$  and  $\alpha_{AFT}$  are winding angles with respect to the forward and the aft polar openings respectively and are defined by

$$\begin{aligned}\alpha_{FWD} &= \sin^{-1} \left( \frac{R_{E\_FWD}}{R} \right) \\ \alpha_{AFT} &= \sin^{-1} \left( \frac{R_{E\_AFT}}{R} \right)\end{aligned}\tag{E.0.3}$$

where  $R_{E\_FWD}$  and  $R_{E\_AFT}$  are radii to the centre of the winding band for the forward and the aft polar openings respectively.

## Appendix F

# Micromechanical Analysis of Laminates

The rule of mixtures is a micro-mechanics analytical method that assumes that:

- The distribution of fibres inside the resin matrix is uniform.
- The bonding fibres-resin is perfect,
- Loads are applied either in the longitudinal direction of the fibres or in their transverse direction.
- The fibre and the resin are linear elastic materials.
- There are no voids in the resin matrix.
- There are initially no residual stresses in constituent materials.

The longitudinal modulus is calculated using the assumption that the strain in the fibre  $\varepsilon_f$ , the strain in the resin matrix  $\varepsilon_m$  and the strain in the composite  $\varepsilon_c$  are the same. This can be seen in Fig. F.1,

$$\varepsilon_f = \varepsilon_m = \varepsilon_c = \frac{\Delta L}{L} \quad (\text{F.0.1})$$

where  $L$  is the initial length of a lamina of the material, and  $\Delta L$  its elongation when a load is applied longitudinally.

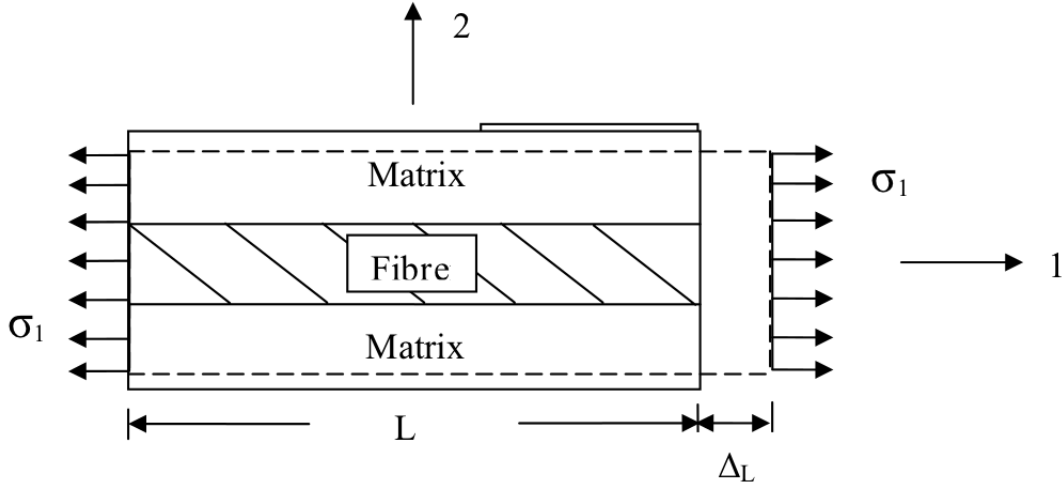


**Figure F.1:** Deformation in longitudinal direction (Yadama and Englund, 2007)

For a static equilibrium, the total force exerted on the composite must be equivalent to the sum of the forces exerted on the fibre and the resin matrix

$$\sigma_{c1}A_c = \sigma_{f1}A_f + \sigma_{m1}A_m \quad (\text{F.0.2})$$

$$\sigma_{c1} = \sigma_{f1}\frac{A_f}{A_c} + \sigma_{m1}\frac{A_m}{A_c} \quad (\text{F.0.3})$$

where  $\sigma_{c1}$ ,  $\sigma_{f1}$ ,  $\sigma_{m1}$  are respectively stresses in the composite, the fibre and the resin matrix and  $A_c$ ,  $A_f$ ,  $A_m$  the corresponding cross sections. Eq. F.0.3 considering the fact that

$$VF_f = \frac{A_f L}{A_c L} = \frac{A_f}{A_c} \quad (\text{F.0.4})$$

$$VF_m = \frac{A_m L}{A_c L} = \frac{A_m}{A_c} \quad (\text{F.0.5})$$

where  $VF_f$  and  $VF_m$  are the volume fractions of the fibre and the resin matrix respectively. Eq F.0.3 becomes

$$\sigma_{c1} = \sigma_{f1}VF_f + \sigma_{m1}VF_m \quad (\text{F.0.6})$$

Taking the Hooke's law into consideration, the equation becomes

$$E_{c1}\varepsilon_c = E_f\varepsilon_f VF_f + E_m\varepsilon_m VF_m \quad (\text{F.0.7})$$

Taking into account the assumption of equal strain expressed by Eq F.0.1, the expression of the longitudinal young modulus is deduced as

$$E_{c1} = E_f VF_f + E_m VF_m = E_f VF_f + E_m(1 - VF_f) \quad (\text{F.0.8})$$

In the transversal direction, the total elongation must be equal to the sum of the elongation of the fibre and the elongation of the matrix, as can be seen in Fig. F.2.

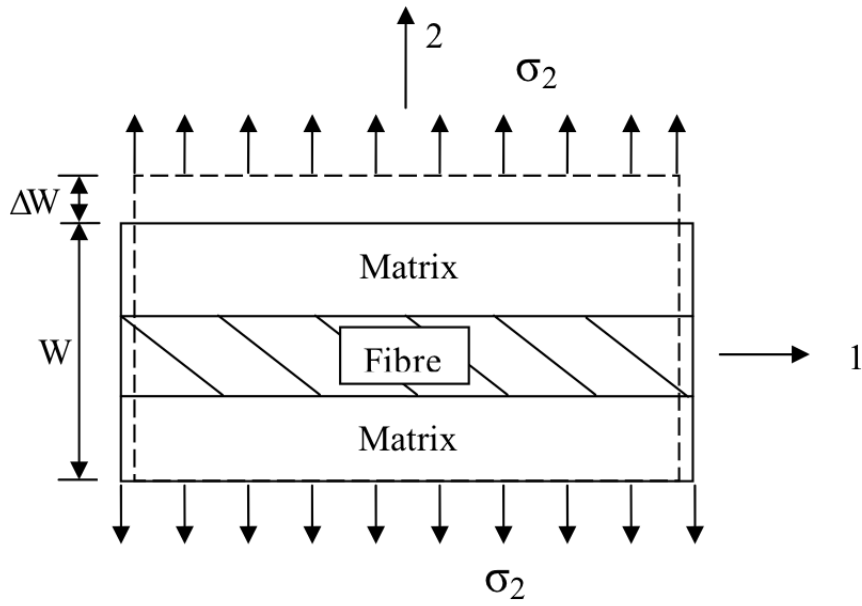


**Figure F.2:** Deformation in transverse direction (Yadama and Englund, 2007)

$$\Delta W = \Delta W_f + \Delta W_m \quad (\text{F.0.9})$$

$$\varepsilon_2 W = \varepsilon_f V F_f W + \varepsilon_m V F_m W \quad (\text{F.0.10})$$

$$\varepsilon_2 = \varepsilon_f V F_f + \varepsilon_m V F_m \quad (\text{F.0.11})$$

$$\frac{\sigma_2}{E_2} = \frac{\sigma_f}{E_f} V F_f + \frac{\sigma_m}{E_m} V F_m \quad (\text{F.0.12})$$

with the assumption the stress is the same in the fibre and in the resin matrix,

$$\frac{1}{E_2} = \frac{V F_f}{E_f} + \frac{V F_m}{E_m} \quad (\text{F.0.13})$$

$$E_2 = \frac{E_f E_m}{E_f V F_m + E_m V F_f} \quad (\text{F.0.14})$$

To establish the expression for the Poisson's ratio let us consider Fig. F.3.

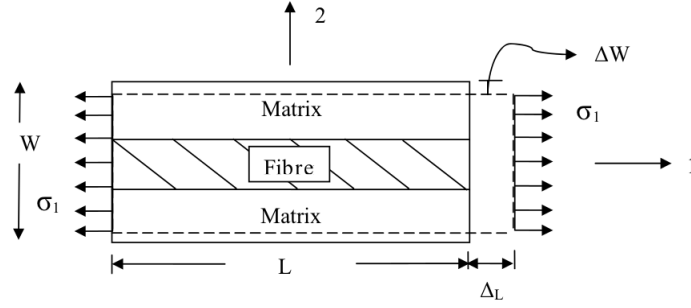


**Figure F.3:** Deformation in a volume element (Yadama and Englund, 2007)

As can be seen,

$$\Delta W = -W\varepsilon_2 = W\nu_{12}\varepsilon_1. \quad (\text{F.0.15})$$

Using micro-mechanics equations

$$\Delta W = \Delta W_f + \Delta W_m \quad (\text{F.0.16})$$

$$\Delta W = WVF_f\nu_f\varepsilon_1 + WVF_m\nu_m\varepsilon_1 \quad (\text{F.0.17})$$

and combining Eq. F.0.15 and Eq. F.0.17 we get,

$$\nu_{12} = \nu_f VF_f + \nu_m VF_m. \quad (\text{F.0.18})$$

To establish the expression of the shear modulus, it is assumed that the shearing stress is the same on the fibre and the matrix as illustrated in Fig. F.4. The total shear deformation

$$\Delta = \Delta_f + \Delta_m \quad (\text{F.0.19})$$

$$\gamma W = VF_f W \gamma_f + VF_m W \gamma_m \quad (\text{F.0.20})$$

$$\gamma = VF_f \gamma_f + VF_m \gamma_m \quad (\text{F.0.21})$$

where  $\gamma$ ,  $\gamma_m$  and  $\gamma_f$  are shear strains in the composite, the fibres and the resin matrix and the fibres respectively.

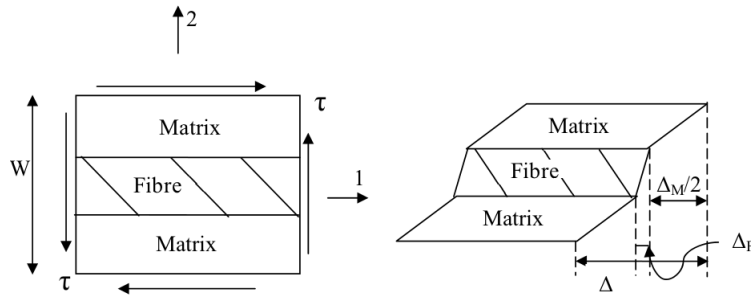


**Figure F.4:** Shearing deformation in a volume element (Yadama and Englund, 2007)

Expressing the shear strain in terms of the shear stress  $\tau$  and the shear modulus, that is

$$\gamma = \frac{\tau}{G_{12}} \quad (\text{F.0.22})$$

Eq. F.0.21 becomes,

$$\frac{\tau}{G_{12}} = VF_f \frac{\tau}{G_f} + VF_m \frac{\tau}{G_m} \quad (\text{F.0.23})$$

where  $G_f$  and  $G_m$  are shear moduli for the fibres and the resin respectively. Therefore,

$$G_{12} = \frac{G_m G_f}{VF_m G_f + VF_f G_m} \quad (\text{F.0.24})$$

The assumption that the stresses in the resin matrix and the fibres are equal is poor and makes the value of the transverse Young's modulus and the in-plane shear modulus obtained using respectively Eq (F.0.14) and Eq (F.0.24) inaccurate. Alternatively these parameters are accurately calculated using other models such as finite element methods, boundary elements methods, variational principal models and others (Kaw, 2006). All these models imply complicated equations. For design use, simple semi-empirical models have been developed. The mostly used semi-empirical models are the Halphin and Tsai models developed by curve fitting to results that are based on elasticity (Kaw, 2006). The transverse Young's modulus equation obtained using the Halphin-Tsai model is

$$E_2 = E_m \frac{1 + \zeta \eta VF_f}{1 - \eta VF_f} \quad (\text{F.0.25})$$

where

$$\eta = \frac{(E_f/E_m) - 1}{(E_f/E_m) + \zeta} \quad (\text{F.0.26})$$

$\zeta$  is referred to as the reinforcing factor, it depends on the fibre geometry, the packing geometry and the loading conditions. As an example, for circular fibres and square packing geometry,  $\zeta = 2$ . In the case of in-plane shear modulus, the Halpin-Tsai semi-empirical model is given by

$$G_{12} = G_m \frac{1 + \zeta \eta VF_f}{1 - \eta VF_f} \quad (\text{F.0.27})$$

where

$$\eta = \frac{(G_f/G_m) - 1}{(G_f/G_m) + \zeta} \quad (\text{F.0.28})$$

$\zeta$  is referred to as the reinforcing factor, it depends on the fibre geometry, the packing geometry and the loading conditions. As an example, for circular fibres and square packing geometry,  $\zeta = 1$ .

# Appendix G

## Genz Algorithm

The Genz algorithm makes it possible to evaluate Eq. 2.3.3 which is the multi-variate normal distribution integral by first transforming the equation into an integral over a unit hyper-cube and then using the simple Monte Carlo method to compute it (Genz, 1992). The transformation is done in three stages. The first stage is a transformation of variables  $\mathbf{g}=(g_1, g_2, \dots, g_n)$  such that  $\mathbf{g} = \mathbf{C}\mathbf{y}$  where  $\mathbf{C}\mathbf{C}^T$  is the Cholesky decomposition (Stewart, 1998) of the correlation matrix  $\mathbf{R}$ . After this transformation, the expression  $\mathbf{g}^T\mathbf{R}^{-1}\mathbf{g}$  in Eq. 2.3.3 becomes,

$$\mathbf{g}^T\mathbf{R}^{-1}\mathbf{g} = \mathbf{y}^T\mathbf{C}^T\mathbf{C}^{-T}\mathbf{C}^{-1}\mathbf{C}\mathbf{y} = \mathbf{y}^T\mathbf{y} \quad (\text{G.0.1})$$

The integral boundaries,  $\boldsymbol{\beta} \leq \mathbf{g} \leq \infty$  become  $\boldsymbol{\beta} \leq \mathbf{C}\mathbf{y} \leq \infty$  then,

$$\boldsymbol{\beta}' \leq \mathbf{y} \leq \infty \quad \text{Where} \quad \beta'_i = \frac{\left( \beta_i - \sum_{j=1}^{i-1} c_{ij}y_j \right)}{c_{ii}} \quad (\text{G.0.2})$$

after the transformation Eq. 2.3.3 becomes,

$$P(F) = \frac{1}{\sqrt{2\pi}^n} \int_{\beta'_1}^{\infty} \exp\left(-\frac{y_1^2}{2}\right) \int_{\beta'_2}^{\infty} \exp\left(-\frac{y_2^2}{2}\right) \dots \int_{\beta'_n}^{\infty} \exp\left(-\frac{y_n^2}{2}\right). \quad (\text{G.0.3})$$

The second stage is the transformation of variables using  $y_i = \Phi^{-1}(z_i)$  where,

$$\Phi(y) = \frac{1}{\sqrt{2\pi}} \int_{-\infty}^y \exp\left(-\frac{\boldsymbol{\theta}^2}{2}\right) d\boldsymbol{\theta} \quad (\text{G.0.4})$$

the integral becomes

$$P(F) = \int_{d_1}^1 \int_{d_2}^1 \dots \int_{d_n}^1 d\mathbf{z} \quad (\text{G.0.5})$$

Where  $d_i = \Phi(\beta'_i)$  and  $1 = \Phi(\infty)$  The last stage is to make the lower limit equal to zero using the transformation  $z_i = d_i + \omega - i(1 - \omega_i)$ . The final integral becomes

$$P(F) = (1 - d_1) \int_0^1 (1 - d_2) \int_0^1 \dots (1 - d_n) \int_0^1 d\boldsymbol{\omega} \quad (\text{G.0.6})$$



where

$$d_i = \Phi \left( \frac{\left( \beta_i - \sum_{j=1}^{i-1} c_{ij} \Phi^{-1}(d_j + \omega_j(1 - d_j)) \right)}{c_{ii}} \right). \quad (\text{G.0.7})$$

The integral G.0.6 can be easily computed using the following simple Monte Carlo algorithm developed by Genz (1992):

1. Input the correlation matrix  $\mathbf{R}$ , the lower integration boundaries which are reliability indices  $\beta_i$  and upper boundaries which are infinity, the tolerance  $\epsilon$ , the Monte Carlo confidence factor for the standard error  $\alpha$  and the maximum number of iterations  $N_{max}$ .

2. Compute the lower triangular Cholesky factor  $\mathbf{C}$  of  $\mathbf{R}$ .

3. Initialise: Probability = 0,  $N = 0$ , Variance = 0,  $d_1 = \Phi \left( \frac{a_1}{c_{1,1}} \right)$  and  $f_1 = 1 - d_1$ .

4. Generate uniform random numbers  $\omega_1, \omega_2, \dots, \omega_{m-1} \in [0, 1]$ .

5. For  $i = 2, 3, \dots, n$ . Set  $y_{i-1} = \Phi^{-1}(d_{i-1} + \omega_{i-1}(1 - d_{i-1}))$ ,

$$d_i = \Phi \left( \frac{a_i - \sum_{j=1}^{i-1} c_{ij} y_j}{c_{ii}} \right) \text{ and } f_i = (1 - d_i) f_{i-1}$$

6. Set  $N = N + 1$ ,  $\delta = \frac{f_m - \text{Probability}}{N}$ , Probability = Probability +  $\delta$ ,  
Variance =  $\frac{(N - 2)\text{Variance}}{N} + \delta^2$  and Error =  $\alpha \sqrt{\text{Variance}}$

7. Repeat 4, 5 and 6 until Error  $\leq \epsilon$  or  $N = N_{max}$ .

8. Return Probability, Error and  $N$ .

# List of References

- Breitung, K. (1984). Asymptotic approximations for multinormal integrals. *Journal of engineering mechanics, ASCE*, vol. 110, no. 3, pp. 357–366.
- Christensen, R. (2005). The comparison and evaluation of three fiber composite failure criteria. *SEM annual conference and exposition on experimental and applied mechanics*.
- Daniel, I.M. and Ishai, O. (2006). *Engineering Mechanics of Composite Materials*. University Press, Oxford.
- Du, X. (2005 September). *Probabilistic Engineering Design*. University of Missouri - Rolla.
- Duell, J.M., Wilson, J. and Kessler, M. (2008). Analysis of a carbon composite overwrap pipeline repair system. *International Journal of Pressure Vessels and Piping*, vol. 85, pp. 782 – 788.
- Genz, A. (1992). Numerical computation fo multivariate normal probabilities. *Journal of Computational and Graphical Statistics*, vol. 1, pp. 141–149.
- Gosavi, M.B., Prof A.S, R. and Patil, V. (2014). A review on failure modes of composite pressure vessel. *International Journal of Engineering Development and Research*, vol. 2.
- Haldar, A. and Mahadevan, S. (2000). *Probability, Reliability and Statistical Methods in Engineering Design*. John Wiley Sons, Inc.
- Hexion (2005 September). *Epon Resin 828 Technical Data Bulletin*.
- Ho, P.Y.-C.L. and Cao, X.-R. (1991 June). Perturbation analysis of discrete event dynamic systems. In: *The Springer International Series in Engineering and Computer Science*, vol. 145. Springer.
- Jianqiao, C., Yuanfu, T., Rui, G., Qunli, A. and Xiwei, G. (2012 March). Reliability design optimization of composite structures based on pso together with fea. *Chine Journal of Aeronautics*, vol. 26, no. 2, pp. 343–349.
- Kabir, M.Z. (2000). Finite element analysis of composite pressure vessels with a load sharing metallic liner. *Composite Structures*, vol. 49, pp. 247 – 255.
- Kaempffert, W. (1919 January). Popular science monthly. Scanned by Google Books. Available at: <http://books.google.com/books?id=HykDAAAAMBAJ&pg=PA13>

- Kaushik, M., John, C., L., T.M., Gri, C., L.J., Chris, P. and S., W.J. (2004 September). Ultralight linerless composite tanks for in-space applications. *Pasadena, CA : Jet Propulsion Laboratory, National Aeronautics and Space Administration, 2004*. Available online on <http://hdl.handle.net/2014/41660>.
- Kaw, A.K. (2006). *Mechanics of Composite Materials, Second Edition*. CRC Press Taylor and Francis Group.
- Kawahara, G. and McCleskey, S.F. (1966 November). Titanium lined, carbon composite overwrapped pressure vessel. *AIAA-ASME-SAE-ASEE Joint Propulsion Conference*, , no. AIAA 96-2751.
- Kumar, S.S. and Kumari, A.S. (2012 September). Design and failure analysis of geodesic dome of a composite pressure vessel. *International Journal of Engineering Research and Technology*, vol. 1, no. 2270-0181.
- Li, K.D.-Q., Jiang1, S.-H., Wu, S.-B., Zhou, C.-B. and Zhang, L.-M. (2013). Monte carlo simulation for structural reliability analysis with complex performance function. *Proceedings of the Institution of Mechanical Engineers, Part O: Journal of Risk and Reliability*, vol. 227, no. 2, pp. 109–118.
- Lorie, G.-L., Leigh, M.P.L.N.P.S. and Ronald, G. (2006 March). A comparison of various stress rupture life models for orbiter composite pressure vessels and confidence intervals. *Pasadena, CA : Jet Propulsion Laboratory, National Aeronautics and Space Administration*. Available online at <http://hdl.handle.net/2014/41496>.
- Madhavi, M., Rao, K. and Rao, K.N. (2009 January). Design and analysis of filament wound composite pressure vessel with integrated-end domes. *Defense Science Journal*, vol. 59, no. 1, pp. 73–81.
- McLaughlan, P.B. and Forth, S.C. (2011 March). Composite overwrapped pressure vessels, a primer. *NASA Scientific and Technical Information (STI)*, , no. NASA/SP-2011-573.
- Mian, H.H., Wang, G., Dar, U.A. and Zhang, W. (2013). Optimization of composite material system and lay-up to achieve minimum weight pressure vessel. *Applied Composite Materials*, vol. 20, pp. 873–889.
- MSC (2012). *MSC Laminate Modeler User's Guide*.
- Murthy, P.L.N. and Phoenix, S.L. (2009). Designing of a fleet-leader program for carbon composite overwrapped pressure vessels. Technical Memorandum NASA/TM-2009-215685, NASA. Available online at <http://gltrs.grc.nasa.gov>.
- Nettles, A.T. and Biss, E.J. (1996). Low temperature mechanical testing of carbon-fiber/epoxy-resin composite materials. Technical Paper 3663, NASA.
- Olsson, A., Sandberg, G. and Dahlblom, O. (2002). On latin hypercube sampling for structural reliability analysis.

- Pat B. McLaughlan, P.E., Forth, S.C. and Grimes-Ledesma, L.R. (2011 March). Composite overwrapped pressure vessels, a primer. Special Publication NASA/SP-2011-573, NASA.
- Peters, S., Green, J.E., Koussios, S., Priestly, A., McLarty, J.L., Leslie, J. and Leynolds, H. (2011 September). *Composite Filament Winding*. ASM International.
- Reeder, J.R. (2012 April). Composite stress rupture: A new reliability model based on strength decay. *NASA Center For AeroSpace Information*, , no. NASA/TM-2012-217566.
- Rosenblatt, M. (1952). Remarks on multivariate transformation. *Annal of Mathematics and Statistics*, vol. 23, no. 3, pp. 470–472.
- Rubinstein, R.Y. and Shapiro, A. (1993). *Sensitivity analysis and stochastic optimization by the score function method*. John Wiley & Sons Ltd.
- SIMULIA (2007). *Wound Composite Modeler For Abaqus User's Manual*. Abaqus Version 6.7-3.
- Stewart, G.W. (1998). *Matrix Algorithms*, vol. 1. Basic Decompositions. Society for Industrial and Applied Mathematics.
- Tam, W.H., Griffin, P.S. and Jackson, A.C. (2002). Design and manufacture of a composite overwrapped pressurant tank assembly. *AIAA*, , no. AIAA 2002-4349.
- Toray (2008). *Torayca T1000G Data Sheet*.
- Vanderplaats, G.N. (1984). *Numerical optimization techniques for engineering design: with applications*. McGraw-Hill Ryerson, Limited.
- Vanderplaats Research & Development, I. (2001). *DOT, Design Optimization Tools, Users Manual Version 5.X*.
- Venter, G. and Scotti, S.J. (2010). Accounting for proof test data in a reliability based design optimization framework.
- Viana, F.A., Venter, G. and Balabanov, V. (). An algorithm for fast optimal latin hypercube design of experiments.
- Wu, E. and Tsai, S. (1971). The tsai-wu failure criterion. *Journal of Composite Materials*, vol. 5, pp. 58–80.
- Yadama, V. and Englund, K. (2007 August). Natural fiber thermoplastic composites. Notes available on Scribd.